

Channel Estimation for IRS-Assisted Millimeter-Wave MIMO Systems: Sparsity-Inspired Approaches

Tian Lin, *Student Member, IEEE*, Xianghao Yu, *Member, IEEE*,
Yu Zhu, *Member, IEEE*, and Robert Schober, *Fellow, IEEE*

Abstract

Due to their ability to create favorable line-of-sight (LoS) propagation environments, intelligent reflecting surfaces (IRSs) are regarded as promising enablers for future millimeter-wave (mm-wave) wireless communication. In this paper, we investigate channel estimation for IRS-assisted mm-wave multiple-input multiple-output (MIMO) wireless systems. By leveraging the sparsity of mm-wave channels in the angular domain, we formulate the channel estimation problem as an ℓ_1 -norm regularized optimization problem with fixed-rank constraints. To tackle the non-convexity of the formulated problem, an efficient algorithm is proposed by capitalizing on alternating minimization and manifold optimization (MO), which yields a locally optimal solution. To further reduce the computational complexity of the estimation algorithm, we propose a compressive sensing- (CS-) based channel estimation approach. In particular, a three-stage estimation protocol is put forward where the subproblem in each stage can be solved via low-complexity CS methods. Furthermore, based on the acquired channel state information (CSI) of the cascaded channel, we design a passive beamforming algorithm for maximization of the spectral efficiency. Simulation results reveal that the proposed MO-based estimation (MO-EST) and beamforming algorithms significantly outperform two benchmark schemes while the CS-based estimation (CS-EST) algorithm strikes a balance between performance and complexity. In addition, we demonstrate the robustness of the MO-EST algorithm with respect to imperfect knowledge of the sparsity level of the channels, which is crucial for practical implementations.

This paper was presented in part at the IEEE Global Communications Conference, Taipei, Taiwan, Dec. 2020 [1].

Tian Lin and Yu Zhu are with the Department of Communication Science and Engineering, Fudan University, Shanghai, China (e-mail: lint17@fudan.edu.cn, zhuyu@fudan.edu.cn).

Xianghao Yu is with the Department of Electronic and Computer Engineering, the Hong Kong University of Science and Technology (HKUST), Kowloon, Hong Kong (e-mail: eexyu@ust.hk).

Robert Schober is with the Institute for Digital Communications, Friedrich-Alexander-University Erlangen-Nuremberg (FAU), 91054 Erlangen, Germany (e-mail: robert.schober@fau.de).

Index Terms

Channel estimation, compressive sensing, fixed-rank manifold optimization, intelligent reflecting surface, MIMO.

I. INTRODUCTION

Due to its enormous potential for overcoming the spectrum crunch, millimeter-wave (mm-wave) communication has been regarded as a key technology for future wireless cellular systems [2], [3]. By leveraging large antenna arrays to synthesize directional beams and exploiting the large available bandwidth, mm-wave communication enables gigabit-per-second data rates [4]. However, mm-wave communication is vulnerable to blockages due to the limited scattering effects at mm-wave frequencies. As the propagation environment of conventional mm-wave communication systems is uncontrollable, the quality of service (QoS) is significantly degraded when line-of-sight (LoS) links are not available.

Recently, intelligent reflecting surfaces (IRSs) have been incorporated into wireless communication systems, mainly due to their capability of customizing favorable wireless propagation environments [5], [6]. Equipped with a large number of low-cost *passive* reflecting elements, e.g., diodes and phase shifters, IRSs enable the adaptation of wireless propagation environments with limited power consumption [7]. This property of IRSs is particularly advantageous for coverage extension of mm-wave wireless systems [8]–[10]. Specifically, when the direct LoS links between the base station (BS) and the user equipments (UEs) are blocked, the deployed IRSs can reflect the incident signals to provide virtual LoS links for mm-wave communications. Furthermore, with well-designed IRS reflecting elements, the communication performance can be further enhanced via programmable and reconfigurable signal reflections. In spite of their great potential, the introduction of IRSs in wireless systems also brings new challenges, among which the acquisition of channel state information (CSI) may be the most difficult task. Although the CSI of the direct BS-UE links can be obtained by turning off the IRSs and applying conventional CSI acquisition approaches, it is difficult to estimate the two IRS-assisted channels, i.e., the BS-IRS channel and IRS-UE channel. In particular, since radio frequency (RF) chains are not available at the passive IRSs, it is not possible to estimate the two IRS-assisted channels directly by regarding the IRS as a conventional RF chain-driven transceiver. Therefore, the classical channel estimation techniques are not applicable to the newly-emerging IRS-assisted communication systems.

Several works have investigated channel estimation in IRS-assisted wireless systems [11]–[21]. The authors of [11], [12] characterized the minimum pilot sequence length for channel estimation in IRS-assisted multi-user multiple-input single-output (MISO) systems based on the least square (LS) criterion. To further reduce the pilot overhead, compressive sensing (CS) techniques were utilized in [13]–[15] to solve the estimation problem based on the assumption that the channel matrices are sparse. However, the algorithms proposed in these works are only applicable in wireless systems with single-antenna UEs, which are unlikely to be used in mm-wave systems. Channel estimation for IRS-assisted multiple-input multiple-output (MIMO) systems was first studied in [16]. A matrix factorization-based algorithm was proposed where during training each reflecting element was turned on successively while keeping the remaining reflecting elements off. In [17], the authors focused on the estimation of the dominant LoS path of IRS-assisted MIMO channels to simplify the channel estimation problem, and an iterative reweighting method based on the gradient descend algorithm was proposed. By modeling the received pilots of IRS-assisted MIMO system as a tensor, a parallel factor decomposition (PARAFAC) algorithm was developed in [18], [19] to estimate the IRS-assisted channels. While these approaches designed for sub-6 GHz bands are also applicable to mm-wave MIMO systems, a significant performance loss is expected as the unique channel characteristics of mm-wave MIMO systems are not taken into account. By exploiting the sparsity of mm-wave channels, the channel estimation for IRS-assisted MIMO mm-wave systems was formulated as a classical sparse signal recovery problem in [20], such that conventional CS techniques, e.g., the orthogonal matching pursuit (OMP) and the generalized approximate message passing (GAMP) algorithms, can be directly applied. In addition, an iterative atom pruning based subspace pursuit (IAP-SP) scheme was developed to solve the sparse signal recovery problem, where the columns of the sensing matrix that are least correlated with the signal residual are eliminated in the iterative process [21]. However, the computational complexity of these CS-based algorithms scales cubically in the number of antennas and the number of reflecting elements [20], [21], which is prohibitively high especially in massive MIMO systems empowered by large-scale IRSs. Therefore, we conclude that efficient channel estimation algorithms for IRS-assisted mm-wave MIMO systems are not available in the literature, yet.

In this paper, we investigate the channel estimation problem of IRS-assisted mm-wave MIMO systems operating in the time division duplex (TDD) mode. The BS and UE are both equipped with multiple antennas, and an IRS consisting of programmable phase shifters is deployed to customize a favorable propagation environment for mm-wave communication. Compared to its

conference version [1], this paper leverages the sparsity of mm-wave channels in the angular domain, based on which the channel estimation problem can be formulated as an ℓ_1 -norm regularized optimization problem with fixed-rank constraints. To tackle the high degree of non-convexity of the formulated problem, we first apply alternating minimization (AM) to decouple the formulated problem into two subproblems, which correspond to the estimation of the UE-IRS channel and the IRS-BS channel, respectively. Subsequently, manifold optimization (MO) is employed to address the fixed-rank constraint in each one of the subproblems, which leads to a locally optimal solution of the channel estimation problem. To further reduce the computational complexity, we propose a channel estimation algorithm based on CS techniques. In particular, we divide the overall estimation phase into three stages, where the subproblem in each stage can be efficiently solved by the OMP method. Finally, with the estimated channel at hand, a novel passive beamforming algorithm for spectral efficiency maximization is developed by solving an equivalent weighted mean square error minimization (WMMSE) problem. Based on the AM principle, closed-form solutions of the beamformers at the BS and UE are derived while the reflection coefficients are optimized via the MO technique. The proposed beamforming algorithm is guaranteed to converge to a locally optimal solution of the WMMSE problem. Simulation results show that the proposed MO-based estimation (MO-EST) algorithm significantly outperforms two benchmark schemes proposed in [18] and [20], respectively. Meanwhile, the CS-based estimation (CS-EST) algorithm strikes a good balance between performance and computational complexity. Besides, we demonstrate the robustness of the proposed estimation algorithms when the channel sparsity levels are not perfectly known. We also reveal the superiority of the proposed beamforming algorithm compared with the state of the art [22], [23].

Notations: In this paper, the imaginary unit of a complex number is denoted by $j = \sqrt{-1}$. The set of nonnegative integers is denoted by $\mathbb{N} = \{0, 1, \dots\}$. $\mathbb{C}^{m \times n}$ denotes the set of all $m \times n$ complex-valued matrices. Matrices and vectors are denoted by boldface capital and lower-case letters, respectively. \mathbf{I}_N denotes the $N \times N$ identity matrix. $\mathbf{1}_N$ denotes the $N \times 1$ all-ones vector. $(\cdot)^*$, $(\cdot)^T$, $(\cdot)^H$, $\text{rank}(\cdot)$, $\text{tr}(\cdot)$, $\text{vec}(\cdot)$, and $\|\cdot\|_F$ denote the conjugate, transpose, conjugate transpose, rank, trace, vectorization, and Frobenius norm of a matrix, respectively. $\|\cdot\|_0$, $\|\cdot\|_1$, and $\|\cdot\|$ represent the ℓ_0 -norm, ℓ_1 -norm, and ℓ_2 -norm of a vector, respectively. The Hadamard, Kronecker, and Khatri-Rao products are represented by \circ , \otimes , and \odot , respectively. $|\cdot|$ denotes the absolute value or the magnitude of a complex number. $d(\cdot)$ denotes the differential, i.e., an infinitesimal difference in calculus. $\Re(\cdot)$ and $\mathbb{E}(\cdot)$ denote the real part of a complex number and statistical expectation, respectively. $\text{diag}(\mathbf{x})$ is a diagonal matrix with the entries of \mathbf{x} on its main

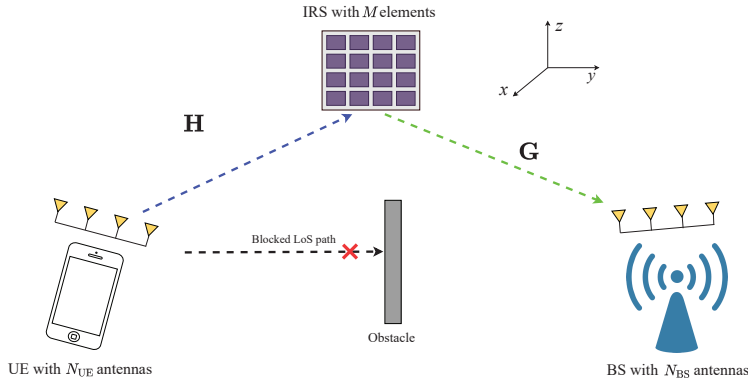


Fig. 1. An uplink IRS-assisted mm-wave MIMO communication system.

diagonal. $\mathcal{CN}(\mathbf{0}, \Sigma)$ denotes the circularly symmetric complex Gaussian distribution with zero mean and covariance matrix Σ . $[\mathbf{A}]_{ij}$ and $[\mathbf{a}]_i$ denote the (i, j) -th entry of matrix \mathbf{A} and the i -th entry of vector \mathbf{a} , respectively.

II. SYSTEM MODEL AND CHANNEL MODEL

A. System Model

We consider uplink channel estimation in an IRS-assisted mm-wave point-to-point MIMO system operating in the TDD mode, as shown in Fig. 1. The UE and the BS are equipped with N_{UE} and N_{BS} antennas, respectively. In addition, one passive IRS employing M phase shifters is deployed to establish a virtual LoS link for the UE that would otherwise be blocked¹. For each block, we assume that the time period available for channel estimation is divided into T time slots. In the t -th time slot, the equivalent baseband received signal $\mathbf{r}_t \in \mathbb{C}^{N_{\text{BS}}}$ at the BS side can be expressed as follows

$$\mathbf{r}_t = \mathbf{G}\Phi_t\mathbf{H}\mathbf{s}_t + \mathbf{z}_t, \quad (1)$$

where $\mathbf{s}_t \in \mathbb{C}^{N_{\text{UE}}}$ denotes the transmit pilot vector in the t -th time slot, which is known at the BS, and the power allocated to the pilot vector is given by $\|\mathbf{s}_t\|^2 = P_{\text{tr}}$. $\mathbf{H} \in \mathbb{C}^{M \times N_{\text{UE}}}$ and $\mathbf{G} \in \mathbb{C}^{N_{\text{BS}} \times M}$ represent the channels from the UE to the IRS and from the IRS to the BS, respectively. \mathbf{z}_t denotes the received additive Gaussian noise vector with $\mathbf{z}_t \sim \mathcal{CN}(\mathbf{0}, \sigma^2 \mathbf{I}_{N_{\text{BS}}})$, where σ^2 represents the noise power. The reflection coefficient matrix of the IRS in the t -th time

¹The proposed scheme can be readily extended to the scenario with LoS links. In particular, we can switch off all the IRS elements [11], then the estimation of the direct UE-BS channel reduces to a conventional MIMO channel estimation problem, which can be efficiently solved via existing algorithms [24].

slot is given by diagonal matrix $\Phi_t = \text{diag}(\mathbf{v}_t)$, where $\mathbf{v}_t \in \mathbb{C}^M$ represents the training reflection coefficient vector. Since the IRS is implemented by phase shifters [25], the reflecting elements can only change the phases of the signals, i.e., $|\mathbf{v}_t[n]| = 1$ for $n = 1, \dots, M$. Finally, the pilots received in all T time slots, i.e., $\mathbf{r}_1, \dots, \mathbf{r}_T$, are collected at the BS for channel estimation.

B. Mm-Wave Channel Model

In this paper, we assume that the UE and the BS are both equipped with uniform linear array (ULA) antennas. As the mm-wave propagation environment is well characterized by the Saleh-Valenzuela model [13], [20], the channel matrices can be modeled as

$$\begin{aligned} \mathbf{G} &= \sqrt{\frac{N_{\text{BS}}M}{P}} \sum_{p=1}^P \alpha_p \mathbf{a}_{\text{BS}}(\theta_r^p) \mathbf{a}_{\text{IRS}}^H(\theta_t^p, \phi_t^p), \\ \mathbf{H} &= \sqrt{\frac{N_{\text{UE}}M}{Q}} \sum_{q=1}^Q \beta_q \mathbf{a}_{\text{IRS}}(\psi_r^q, \varphi_r^q) \mathbf{a}_{\text{UE}}^H(\psi_t^q), \end{aligned} \quad (2)$$

where α_p , θ_r^p , and θ_t^p (ϕ_t^p) denote the complex gain, angle of arrival (AoA), and azimuth (elevation) angle of departure (AoD) of the p -th path of the IRS-BS channel. Similarly, β_q , ψ_r^q (φ_r^q), and ψ_t^q denote the complex gain, azimuth (elevation) AoA, and AoD of the q -th path of the UE-IRS channel. In addition, P and Q denote the numbers of paths of the IRS-BS channel and the UE-IRS channel, respectively. Besides, \mathbf{a}_{BS} , \mathbf{a}_{IRS} , and \mathbf{a}_{UE} denote the receive and transmit array response vectors at the BS, IRS, and UE, respectively. Specifically, define

$$\mathbf{f}(u, N) = \frac{1}{\sqrt{N}} [1, e^{j\pi u}, \dots, e^{j\pi(N-1)u}]^T. \quad (3)$$

Then, the array response vectors of the half-wavelength spaced ULAs at the BS and UE are given by

$$\mathbf{a}_{\text{BS}}(\theta_r^p) = \mathbf{f}(\cos(\theta_r^p), N_{\text{BS}}) \quad \text{and} \quad \mathbf{a}_{\text{UE}}(\psi_t^q) = \mathbf{f}(\cos(\psi_t^q), N_{\text{UE}}), \quad (4)$$

respectively. In addition, the array response vector of the IRS involving $M_z \times M_y$ ($M \triangleq M_y M_z$) elements is given by

$$\mathbf{a}_{\text{IRS}}(\theta, \phi) = \mathbf{a}_y(\theta, \phi) \otimes \mathbf{a}_z(\phi), \quad (5)$$

where $\mathbf{a}_y(\theta, \phi) = \mathbf{f}(\sin \theta \sin \phi, M_y)$, $\mathbf{a}_z(\phi) = \mathbf{f}(\cos \phi, M_z)$.

Remark 1: In Sections III and IV, the numbers of paths P and Q are assumed to be known at the BS. In practice, they can be estimated by classical direction-of-arrival (DOA) estimation methods, e.g., multiple signal classification (MUSIC) and estimation of signal parameters via rotational invariant techniques (ESPRIT). In Section VI, we shall consider the case where P and

Q are not accurately known to test the robustness of the proposed algorithms with respect to a mismatched number of paths.

C. Sparse Representation of Mm-Wave Channel

Considering the described channel model, the two IRS-assisted mm-wave channel matrices to be estimated can be rewritten in an angular domain representation as follows [13], [20]

$$\mathbf{H} = \mathbf{A}_I \mathbf{\Lambda}_H \mathbf{A}_{UE}^H, \quad \mathbf{G} = \mathbf{A}_{BS} \mathbf{\Lambda}_G \mathbf{A}_I^H, \quad (6)$$

where $\mathbf{A}_I \in \mathbb{C}^{M \times G_I}$, $\mathbf{A}_{UE} \in \mathbb{C}^{N_{UE} \times G_{UE}}$, and $\mathbf{A}_{BS} \in \mathbb{C}^{N_{BS} \times G_{BS}}$ are three overcomplete dictionary matrices in the angular domain consisting of array response vectors, each of which corresponds to one specific AoA/AoD at the IRS, UE, and BS, respectively [13]. Here, G_I , G_{UE} , and G_{BS} represent the corresponding angular resolutions. Thus, $\mathbf{\Lambda}_G \in \mathbb{C}^{G_{BS} \times G_I}$ and $\mathbf{\Lambda}_H \in \mathbb{C}^{G_I \times G_{UE}}$ are two angular domain sparse matrices with P and Q non-zero elements corresponding to the channel path gains $\{\alpha_p\}$ and $\{\beta_q\}$ in (2), respectively [21], [26]. Specifically, according to (4), the dictionary matrices \mathbf{A}_{BS} and \mathbf{A}_{UE} are given by

$$\begin{aligned} \mathbf{A}_{BS} &= \left[\mathbf{f}(-1, N_{BS}), \mathbf{f}\left(-1 + \frac{2}{G_{BS}}, N_{BS}\right), \dots, \mathbf{f}\left(1 - \frac{2}{G_{BS}}, N_{BS}\right) \right], \\ \mathbf{A}_{UE} &= \left[\mathbf{f}(-1, N_{UE}), \mathbf{f}\left(-1 + \frac{2}{G_{UE}}, N_{UE}\right), \dots, \mathbf{f}\left(1 - \frac{2}{G_{UE}}, N_{UE}\right) \right]. \end{aligned} \quad (7)$$

Similarly, according to (5), the dictionary matrix \mathbf{A}_I is given by

$$\mathbf{A}_I = \mathbf{A}_y \otimes \mathbf{A}_z, \quad (8)$$

where $\mathbf{A}_y = [\mathbf{f}(-1, M_y), \mathbf{f}(-1 + \frac{2}{G_y}, M_y), \dots, \mathbf{f}(1 - \frac{2}{G_y}, M_y)]$ and $\mathbf{A}_z = [\mathbf{f}(-1, M_z), \mathbf{f}(-1 + \frac{2}{G_z}, M_z), \dots, \mathbf{f}(1 - \frac{2}{G_z}, M_z)]$. Here, G_y and G_z denote the angular resolutions along the y - and z -axes, respectively, such that $G_I = G_y G_z$.

III. PROPOSED MO-EST ALGORITHM

In this section, we first exploit the sparsity of mm-wave channels and formulate the estimation problem. Then, by capitalizing on the AM and MO techniques, we develop the MO-EST algorithm to efficiently obtain a locally optimal solution for the formulated estimation problem.

A. Estimation Problem Formulation

According to [12], the minimum variance unbiased estimators of \mathbf{H} and \mathbf{G} can be obtained based on the LS criterion. Thus, based on the system model elaborated in Section II, the LS estimators of the channels can be obtained by solving the following problem

$$\underset{\hat{\mathbf{G}}, \hat{\mathbf{H}}}{\text{minimize}} \quad \sum_{t=1}^T \|\mathbf{r}_t - \hat{\mathbf{G}}\Phi_t\hat{\mathbf{H}}\mathbf{s}_t\|^2, \quad (9)$$

where $\hat{\mathbf{G}}$ and $\hat{\mathbf{H}}$ denote the estimates of \mathbf{G} and \mathbf{H} , respectively. Note that this LS formulation holds for any IRS-assisted wireless system. However, directly solving problem (9) does not leverage the special properties of mm-wave channels, which inevitably leads to a significant performance loss [1]. Besides, $T \geq MN_{\text{UE}}$ is required to guarantee a unique solution of problem (9) [12], [18]. In other words, the training overhead becomes prohibitive for large numbers of antennas and reflecting elements. Therefore, before formulating the channel estimation problem, we explicitly exploit two unique properties of mm-wave channels in the following two lemmas.

Lemma 1 *Suppose $\min(N_{\text{BS}}, M) \geq P$ and $\min(N_{\text{UE}}, M) \geq Q$, then we have*

$$\text{rank}(\mathbf{G}) = P, \quad \text{rank}(\mathbf{H}) = Q. \quad (10)$$

Proof: Please refer to Appendix A. ■

Lemma 1 indicates that mm-wave channels have a fixed low rank, i.e., the channel matrices are sparse in their eigenvalues. It was shown in [1] that mm-wave channels can be effectively estimated by leveraging their low-rank property. However, the consideration of the low-rank constraint in estimation problem (9) does not reduce the exceedingly large training overhead, i.e., we still need $T \geq MN_{\text{UE}}$. Therefore, we also exploit another crucial property of mm-wave channels. Based on the angular domain representation of \mathbf{H} and \mathbf{G} in Section II-C, we present the following lemma.

Lemma 2 *By setting $G_{\text{I}} = M$, $G_{\text{UE}} = N_{\text{UE}}$, and $G_{\text{BS}} = N_{\text{BS}}$, the two ℓ_0 -norms related to the estimated channels are asymptotically given by*

$$\|\boldsymbol{\lambda}_{\mathbf{H}}\|_0 = Q, \quad \|\boldsymbol{\lambda}_{\mathbf{G}}\|_0 = P, \quad (11)$$

where $\boldsymbol{\lambda}_{\mathbf{H}} \triangleq \text{vec}(\mathbf{A}_{\text{I}}^H \mathbf{H} \mathbf{A}_{\text{UE}})$ and $\boldsymbol{\lambda}_{\mathbf{G}} \triangleq \text{vec}(\mathbf{A}_{\text{BS}}^H \mathbf{G} \mathbf{A}_{\text{I}})$.

Proof: Notice that when $G_{\text{I}} = M$, $G_{\text{UE}} = N_{\text{UE}}$, and $G_{\text{BS}} = N_{\text{BS}}$, \mathbf{A}_{BS} , \mathbf{A}_{UE} , and \mathbf{A}_{I} are all unitary matrices according to (7) and (8). Therefore, we have $\mathbf{A}_{\text{I}}^H \mathbf{H} \mathbf{A}_{\text{UE}} = \boldsymbol{\Lambda}_{\mathbf{H}}$ and $\mathbf{A}_{\text{BS}}^H \mathbf{G} \mathbf{A}_{\text{I}} = \boldsymbol{\Lambda}_{\mathbf{G}}$. According to the sparse representation of mm-wave channels in Section II-C, $\boldsymbol{\Lambda}_{\mathbf{G}}$ and $\boldsymbol{\Lambda}_{\mathbf{H}}$

are sparse matrices with P and Q non-zero elements, respectively, which completes the proof of Lemma 2. \blacksquare

Recall that Lemma 1 reveals the low-rank property of the channels themselves. In contrast, Lemma 2 indicates that there is another essential uniqueness, i.e., sparsity, inherited in the angular domain representations. By exploiting Lemmas 1 and 2, we refine estimation problem (9) as follows

$$\begin{aligned} & \underset{\hat{\mathbf{G}}, \hat{\mathbf{H}}}{\text{minimize}} && \sum_{t=1}^T \|\mathbf{r}_t - \hat{\mathbf{G}}\Phi_t\hat{\mathbf{H}}\mathbf{s}_t\|^2 \\ & \text{subject to} && \text{rank}(\hat{\mathbf{G}}) = P, \quad \text{rank}(\hat{\mathbf{H}}) = Q, \\ & && \|\boldsymbol{\lambda}_{\hat{\mathbf{G}}}\|_0 = P, \quad \|\boldsymbol{\lambda}_{\hat{\mathbf{H}}}\|_0 = Q, \end{aligned} \quad (12)$$

where $\boldsymbol{\lambda}_{\hat{\mathbf{H}}} \triangleq \text{vec}(\mathbf{A}_I^H \hat{\mathbf{H}} \mathbf{A}_{\text{UE}})$ and $\boldsymbol{\lambda}_{\hat{\mathbf{G}}} \triangleq \text{vec}(\mathbf{A}_{\text{BS}}^H \hat{\mathbf{G}} \mathbf{A}_I)$. Unfortunately, problem (12) is intractable due to the highly non-convex constraints. Hence, a globally optimal solution cannot be obtained in general. To tackle the non-convex ℓ_0 -norm constraints introduced by the low-rank and sparse properties of mm-wave channels, we resort to the ℓ_1 -norm regularization approach. In particular, the cardinality constraint induced by the ℓ_0 -norm is relaxed by its convex envelop, i.e., the ℓ_1 -norm [27]. In addition, the regularized terms are scaled by tuning parameters to avoid over-fitting. Correspondingly, the estimation problem (12) is reformulated as follows

$$\begin{aligned} & \underset{\hat{\mathbf{G}}, \hat{\mathbf{H}}}{\text{minimize}} && f = \sum_{t=1}^T \|\mathbf{r}_t - \hat{\mathbf{G}}\Phi_t\hat{\mathbf{H}}\mathbf{s}_t\|^2 + \mu_{\mathbf{G}}\|\boldsymbol{\lambda}_{\hat{\mathbf{G}}}\|_1 + \mu_{\mathbf{H}}\|\boldsymbol{\lambda}_{\hat{\mathbf{H}}}\|_1 \\ & \text{subject to} && \text{rank}(\hat{\mathbf{G}}) = P, \quad \text{rank}(\hat{\mathbf{H}}) = Q, \end{aligned} \quad (13)$$

where $\mu_{\mathbf{G}}$ and $\mu_{\mathbf{H}}$ denote the tuning parameters that control the sparsity levels of $\boldsymbol{\lambda}_{\hat{\mathbf{G}}}$ and $\boldsymbol{\lambda}_{\hat{\mathbf{H}}}$, respectively.

Problem (13) is still difficult to solve due to the coupled optimization variables in the objective function f and the highly non-convex low-rank constraints. Therefore, we decouple the optimization of the two variables in problem (13) by applying the AM principle, which has been widely adopted in different wireless communication application scenarios, e.g., hybrid precoding for massive MIMO systems [28] and passive beamforming for IRS-assisted systems [29], [30]. Specifically, we first fix $\hat{\mathbf{H}}$ and minimize f with respect to $\hat{\mathbf{G}}$. The subproblem is given by

$$\begin{aligned} & \underset{\mathbf{X}}{\text{minimize}} && f_1 = \|\mathbf{R} - \mathbf{X}\mathbf{F}\|_F^2 + \mu_{\mathbf{G}}\|\boldsymbol{\lambda}_{\mathbf{X}}\|_1 \\ & \text{subject to} && \text{rank}(\mathbf{X}) = P, \end{aligned} \quad (14)$$

where $\mathbf{R} = [\mathbf{r}_1, \dots, \mathbf{r}_T] \in \mathbb{C}^{N_{\text{BS}} \times T}$, $\mathbf{F} = [\Phi_1 \hat{\mathbf{H}} \mathbf{s}_1, \dots, \Phi_T \hat{\mathbf{H}} \mathbf{s}_T] \in \mathbb{C}^{M \times T}$, and $\mathbf{X} \triangleq \hat{\mathbf{G}}$ are defined for notational convenience. To address the non-convex fixed-rank constraint, we apply the MO technique to solve problem (14) in the following.

B. Preliminaries of MO

By extending the definition of the real-valued fixed-rank manifold [31] to the complex domain, the feasible set of problem (14) can be represented as a typical Riemannian manifold [16]

$$\mathcal{M}_P \triangleq \{\mathbf{X} \in \mathbb{C}^{N_{\text{BS}} \times M} : \text{rank}(\mathbf{X}) = P\}, \quad (15)$$

to which optimization tools developed for the Euclidean space, e.g., the gradient descend and trust-region methods, can be transplanted [31], [32]. Before deriving the proposed algorithm, we first introduce some key operations that are necessary for the Riemannian optimization method for \mathcal{M}_P .

1) *Inner product*: By endowing the complex space $\mathbb{C}^{N_{\text{BS}} \times M}$ with the Euclidean metric, the standard inner product between two points $\mathbf{X}_1, \mathbf{X}_2 \in \mathcal{M}_P$ is defined as follows

$$\langle \mathbf{X}_1, \mathbf{X}_2 \rangle = \Re \{ \text{tr}(\mathbf{X}_1^H \mathbf{X}_2) \}. \quad (16)$$

2) *Tangent space*: For a point $\mathbf{X} \in \mathcal{M}_P$ on the manifold, its tangent space $T_{\mathbf{X}}\mathcal{M}_P$, which is composed of all the vectors that tangentially pass through \mathbf{X} , is given by [31]

$$T_{\mathbf{X}}\mathcal{M}_P \triangleq \{\mathbf{X}_U \mathbf{M} \mathbf{X}_V^H + \mathbf{U}_p \mathbf{X}_V^H + \mathbf{X}_U \mathbf{V}_p^H\}, \quad (17)$$

where $\mathbf{X}_U \in \mathbb{C}^{N_{\text{BS}} \times P}$ and $\mathbf{X}_V \in \mathbb{C}^{M \times P}$ denote the semi-unitary matrices containing the first P left and right singular vectors of \mathbf{X} , respectively. $\mathbf{M} \in \mathbb{C}^{P \times P}$ is an arbitrary matrix. In addition, $\mathbf{U}_p \in \mathbb{C}^{N_{\text{BS}} \times P}$ and $\mathbf{V}_p \in \mathbb{C}^{M \times P}$ lie in the null spaces of \mathbf{X}_U and \mathbf{X}_V , respectively, i.e., $\mathbf{U}_p^H \mathbf{X}_U = \mathbf{0}$ and $\mathbf{V}_p^H \mathbf{X}_V = \mathbf{0}$.

3) *Orthogonal projection*: The orthogonal projection of $\mathbf{J} \in \mathbb{C}^{N_{\text{BS}} \times M}$ onto the tangent space of \mathbf{X} , i.e., $T_{\mathbf{X}}\mathcal{M}_P$, is given by

$$\text{Proj}_{\mathbf{X}}(\mathbf{J}) = \mathbf{P}_U \mathbf{J} \mathbf{P}_V + \mathbf{P}_U^\perp \mathbf{J} \mathbf{P}_V + \mathbf{P}_U \mathbf{J} \mathbf{P}_V^\perp, \quad (18)$$

where $\mathbf{P}_U = \mathbf{X}_U \mathbf{X}_U^H$, $\mathbf{P}_V = \mathbf{X}_V \mathbf{X}_V^H$, $\mathbf{P}_U^\perp = \mathbf{I}_{N_{\text{BS}}} - \mathbf{P}_U$, and $\mathbf{P}_V^\perp = \mathbf{I}_M - \mathbf{P}_V$ [31].

C. Conjugate Gradient Method on \mathcal{M}_P

With the basic definitions of the key operations on \mathcal{M}_P at hand, we can formulate the counterpart of the classic conjugate gradient (CG) algorithm in the Euclidean space on the manifold \mathcal{M}_P [31], [32]. The main idea is illustrated in Fig. 2. Specifically, in the i -th iteration initialized at the point $\mathbf{X}_i \in \mathcal{M}_P$, by introducing the definition of the linear space $T_{\mathbf{X}_i}\mathcal{M}_P$, the conventional CG algorithm applicable in the Euclidean space can be applied to find a local

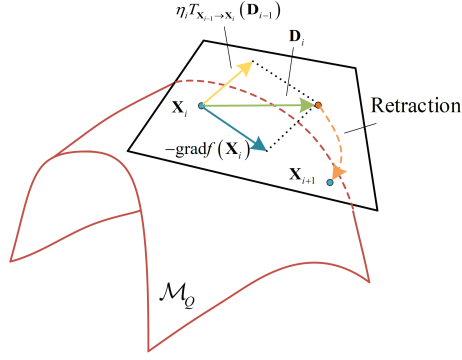


Fig. 2. Illustration of the generalized CG method for the fixed-rank manifold.

minimizer in the tangent space, which is subsequently mapped back to \mathcal{M}_P to obtain \mathbf{X}_{i+1} . For problem (14), the update rule of the search direction of the CG method in the tangent space $T_{\mathbf{X}_i}$ is given by

$$\mathbf{D}_i = -\text{grad}f_1(\mathbf{X}_i) + \eta_i T_{\mathbf{X}_{i-1} \rightarrow \mathbf{X}_i}(\mathbf{D}_{i-1}), \quad (19)$$

where the first term of (19) is the negative Riemannian gradient representing the steepest descent direction of the objective function f_1 in the tangent space $T_{\mathbf{X}_i}\mathcal{M}_P$, and η_i represents the chosen Polak-Ribiere parameter [33, p. 42]. Since the conjugate direction in the previous iteration \mathbf{D}_{i-1} does not lie in $T_{\mathbf{X}_i}\mathcal{M}_P$, the summation in (19) can not be performed directly. To this end, we introduce the *vector transport* operation to project \mathbf{D}_{i-1} to the current tangent space $T_{\mathbf{X}_i}\mathcal{M}_P$. According to (18), the vector transport for \mathcal{M}_P is given by

$$T_{\mathbf{X}_{i-1} \rightarrow \mathbf{X}_i} = \text{Proj}_{\mathbf{X}_i}(\mathbf{D}_{i-1}). \quad (20)$$

Therefore, the remaining task to determine the conjugate direction in (19) is to derive the Riemannian gradient. Since \mathcal{M}_P is embedded in $\mathbb{C}^{N_{\text{BS}} \times M}$, the Riemannian gradient is obtained by projecting the conjugate Euclidean gradient $\nabla_{\mathbf{X}_i^*} f_1$ onto the tangent space [32], i.e.,

$$\text{grad}f_1(\mathbf{X}_i) = \text{Proj}_{\mathbf{X}_i}(\nabla_{\mathbf{X}_i^*} f_1), \quad (21)$$

where $\nabla_{\mathbf{X}_i^*} f_1$ is given by the following lemma.

Lemma 3 *The Euclidean gradient of function f_1 with respect to \mathbf{X}_i^* is given by*

$$\nabla_{\mathbf{X}_i^*} f_1 = -\mathbf{R}\mathbf{F}^H + \mathbf{X}\mathbf{F}\mathbf{F}^H + \frac{\mu\mathbf{G}}{2}\mathbf{A}_{\text{BS}}\mathbf{Y}\mathbf{A}_{\text{I}}^H, \quad (22)$$

where \mathbf{Y} is computed as

$$[\mathbf{Y}]_{ij} = \frac{[\mathbf{A}_{\text{BS}}^H \mathbf{X} \mathbf{A}_{\text{I}}]_{ij}}{|[\mathbf{A}_{\text{BS}}^H \mathbf{X} \mathbf{A}_{\text{I}}]_{ij}|}. \quad (23)$$

Algorithm 1 CG-MO Algorithm

- 1: Randomly initialize $\mathbf{X}_0 \in \mathcal{M}_P$, set $i = 0$ and $f_0 = f_1(\mathbf{X}_0)$.
 - 2: **repeat**
 - 3: Compute the conjugate Euclidean gradient $\nabla_{\mathbf{X}_i^*} f_1$ according to (22);
 - 4: Determine the Riemannian gradient $\text{grad} f_1(\mathbf{X}_i)$ according to (21);
 - 5: Choose Polak-Ribiere parameter η_i [33, p. 42] and obtain the conjugate search direction according to (19);
 - 6: Find \mathbf{X}_{i+1} via retraction (25);
 - 7: $i \leftarrow i + 1$;
 - 8: $f_i = f_1(\mathbf{X}_i)$;
 - 9: **until** $f_{i-1} - f_i \leq \epsilon_1$.
-

Proof: Please refer to Appendix B. ■

Finally, based on the derived search direction \mathbf{D}_i , an operation called *retraction* is introduced to find the destination on the manifold. Specifically, after moving forward along the search direction \mathbf{D}_i in the tangent space, we map the resulting point back to \mathcal{M}_P itself by solving the following optimization problem [31]

$$\mathcal{R}_{\mathbf{X}_i}(\kappa_i \mathbf{D}_i) = \arg \min_{\hat{\mathbf{X}} \in \mathcal{M}_P} \|\mathbf{X}_i + \kappa_i \mathbf{D}_i - \hat{\mathbf{X}}\|^2, \quad (24)$$

where κ_i denotes the Armijo backtracking step size in the i -th iteration [33, Eq. (59)]. A closed-form solution of problem (24) can be obtained via a truncated singular value decomposition (SVD)

$$\mathcal{R}_{\mathbf{X}_i}(\kappa_i \mathbf{D}_i) = \sum_{i=1}^P \zeta_i \mathbf{u}_i \mathbf{q}_i^H, \quad (25)$$

where ζ_i , \mathbf{u}_i , and \mathbf{q}_i are the ordered singular values, left singular vectors, and right singular vectors of $\mathbf{X}_i + \kappa_i \mathbf{D}_i$, respectively. The proposed generalized CG method for the fixed-rank manifold, referred to as the **CG-MO algorithm**, is summarized in **Algorithm 1**, where ϵ_1 is the convergence threshold. We note that the retraction in (25) can be obtained via QR factorization [31]. Hence, the computational complexity of the **CG-MO algorithm** is given by $\mathcal{O}((M + N_{\text{BS}}) P^2)$.

D. Estimation of \mathbf{H}

In this subsection, we consider the optimization of $\hat{\mathbf{H}}$ for given $\hat{\mathbf{G}}$. The corresponding subproblem is obtained as follows

$$\begin{aligned} & \underset{\hat{\mathbf{H}}}{\text{minimize}} && f_2 = \sum_{t=1}^T \|\mathbf{r}_t - \hat{\mathbf{G}}\Phi_t\hat{\mathbf{H}}\mathbf{s}_t\|^2 + \mu_{\mathbf{H}}\|\boldsymbol{\lambda}_{\hat{\mathbf{H}}}\|_1 \\ & \text{subject to} && \text{rank}(\hat{\mathbf{H}}) = Q. \end{aligned} \quad (26)$$

Notice that the feasible set of problem (26) is also a fixed-rank Riemannian manifold, i.e., $\mathcal{M}_Q \triangleq \{\mathbf{X} \in \mathbb{C}^{M \times N_{\text{UE}}} : \text{rank}(\mathbf{X}) = Q\}$ and thus the **CG-MO algorithm** is also applicable. The main modification compared to the optimization of $\hat{\mathbf{G}}$ is the replacement of the conjugate Euclidean gradient in (22) by the conjugate Euclidean gradient of f_2 with respect to $\hat{\mathbf{H}}$, which is given by

$$\nabla_{\hat{\mathbf{H}}^*} f_2 = \frac{\mu_{\hat{\mathbf{H}}}}{2} \mathbf{A}_{\text{I}} \mathbf{Y}_2 \mathbf{A}_{\text{UE}}^H + \sum_{t=1}^T \left(-\Phi_t^H \hat{\mathbf{G}}^H \mathbf{r}_t \mathbf{s}_t^H + \Phi_t^H \hat{\mathbf{G}}^H \hat{\mathbf{G}} \Phi_t \hat{\mathbf{H}} \mathbf{s}_t \mathbf{s}_t^H \right), \quad (27)$$

where \mathbf{Y}_2 is given by

$$[\mathbf{Y}_2]_{ij} = \frac{[\mathbf{A}_{\text{I}}^H \hat{\mathbf{H}} \mathbf{A}_{\text{UE}}]_{ij}}{|[\mathbf{A}_{\text{I}}^H \hat{\mathbf{H}} \mathbf{A}_{\text{UE}}]_{ij}|}. \quad (28)$$

The derivation of (27) is similar to that of (22), and thus, it is omitted here. The resulting overall estimation scheme is referred to as the **MO-EST algorithm**, which is summarized in **Algorithm 2**, where ϵ_2 is the convergence threshold. With the proposed algorithm, the objective values f achieved by the sequence $\left\{ \hat{\mathbf{H}}^{(k)}, \hat{\mathbf{G}}^{(k)} \right\}_{k \in \mathbb{N}}$ form a non-increasing sequence that converges to a stationary value, and any limit point of the sequence $\left\{ \hat{\mathbf{H}}^{(k)}, \hat{\mathbf{G}}^{(k)} \right\}_{k \in \mathbb{N}}$ is a stationary point of problem (13) [32].

Although the proposed MO-EST algorithm has a lower computational complexity than the schemes in [20] and [21], its computational complexity is still relatively high. Specifically, in each iteration of the MO algorithm, the computational complexities of the conjugate gradient and the truncated SVD are $\mathcal{O}(MN_{\text{BS}}(M+N_{\text{UE}}+T))$ and $\mathcal{O}(MN_{\text{BS}}^2 + MN_{\text{UE}}^2)$, respectively. Nevertheless, as will be shown in Section VI, the MO-EST algorithm can serve as a performance upper bound for channel estimation in IRS-assisted mm-wave MIMO systems. Besides, although it is difficult to analytically characterize the training overhead required for the MO-EST algorithm, our simulation results in Section VI show that the MO-EST algorithm significantly reduces the training overhead when compared with conventional LS based channel algorithms [1], [18].

Algorithm 2 MO-EST Algorithm

- 1: Randomly initialize $\hat{\mathbf{G}}^{(0)} \in \mathcal{M}_P$ and $\hat{\mathbf{H}}^{(0)} \in \mathcal{M}_Q$, set $k = 0$, and $f^{(0)} = f(\hat{\mathbf{H}}^{(0)}, \hat{\mathbf{G}}^{(0)})$.
 - 2: **repeat**
 - 3: $k \leftarrow k + 1$;
 - 4: Optimize $\hat{\mathbf{G}}^{(k)}$ for given $\hat{\mathbf{H}}^{(k-1)}$ by solving problem (14) with the CG-MO algorithm;
 - 5: Optimize $\hat{\mathbf{H}}^{(k)}$ for given $\hat{\mathbf{G}}^{(k)}$ by solving problem (26) with the CG-MO algorithm;
 - 6: $f^{(k)} = f(\hat{\mathbf{H}}^{(k)}, \hat{\mathbf{G}}^{(k)})$;
 - 7: **until** $f^{(k-1)} - f^{(k)} \leq \epsilon_2$;
 - 8: Update $\hat{\mathbf{G}}^{(k)}$ and $\hat{\mathbf{H}}^{(k)}$ as the estimates of \mathbf{G} and \mathbf{H} .
-

IV. PROPOSED CS-EST ALGORITHM

To further reduce the computational complexity of channel estimation, in this section, we propose a low-complexity CS-based algorithm as an alternative. Recall that the sparse mm-wave channel representation in Section II-B has three key components, namely the AoAs, AoDs, and the complex gains. Therefore, different from the MO-EST algorithm that directly estimates the channel matrices, the proposed CS-based algorithm recovers the channel matrices by estimating the three associated key components instead.

A. Conventional CS-Based Approach

The received pilot signal in the t -th time slot in (1) can be rewritten as

$$\mathbf{r}_t = (\mathbf{s}_t^T \otimes \mathbf{I}_{N_{\text{BS}}}) (\mathbf{H}^T \odot \mathbf{G}) \mathbf{v}_t + \mathbf{z}_t, \quad (29)$$

where we exploited $\text{vec}(\mathbf{ABC}) = (\mathbf{C}^T \otimes \mathbf{A})\text{vec}(\mathbf{B})$ and $\text{vec}(\mathbf{ADC}) = (\mathbf{C}^T \odot \mathbf{A})\mathbf{d}$, which hold for arbitrary matrices \mathbf{A} , \mathbf{B} , \mathbf{C} . Furthermore, \mathbf{d} denotes the vector of diagonal elements of an arbitrary diagonal matrix \mathbf{D} , i.e., $\mathbf{D} = \text{diag}(\mathbf{d})$. Substituting the angular domain representation (6) into (29), we have

$$\begin{aligned} \mathbf{r}_t &= (\mathbf{s}_t^T \otimes \mathbf{I}_{N_{\text{BS}}}) \left((\mathbf{A}_{\text{UE}}^* \Lambda_{\mathbf{H}}^T \mathbf{A}_{\text{I}}^T) \odot (\mathbf{A}_{\text{BS}} \Lambda_{\mathbf{G}} \mathbf{A}_{\text{I}}^H) \right) \mathbf{v}_t + \mathbf{z}_t \\ &\stackrel{(a)}{=} (\mathbf{s}_t^T \otimes \mathbf{I}_{N_{\text{BS}}}) (\mathbf{A}_{\text{UE}}^* \otimes \mathbf{A}_{\text{BS}}) (\Lambda_{\mathbf{H}}^T \otimes \Lambda_{\mathbf{G}}) (\mathbf{A}_{\text{I}}^T \odot \mathbf{A}_{\text{I}}^H) \mathbf{v}_t + \mathbf{z}_t \\ &= \underbrace{(\mathbf{v}_t^T \otimes \mathbf{s}_t^T \otimes \mathbf{I}_{N_{\text{BS}}}) \left((\mathbf{A}_{\text{I}}^T \odot \mathbf{A}_{\text{I}}^H)^T \otimes (\mathbf{A}_{\text{UE}}^* \otimes \mathbf{A}_{\text{BS}}) \right)}_{\Psi_t} \underbrace{\text{vec}(\Lambda_{\mathbf{H}}^T \otimes \Lambda_{\mathbf{G}})}_{\boldsymbol{\mu}} + \mathbf{z}_t, \end{aligned} \quad (30)$$

where (a) follows from $(\mathbf{AB}) \odot (\mathbf{CD}) = (\mathbf{A} \otimes \mathbf{C})(\mathbf{B} \odot \mathbf{D})$ and $\boldsymbol{\mu} \in \mathbb{C}^{G_{\text{UE}} G_{\text{BS}} G_{\text{I}}^2}$ is a sparse vector with PQ non-zero elements. According to (30), the overall received pilots in T successive time

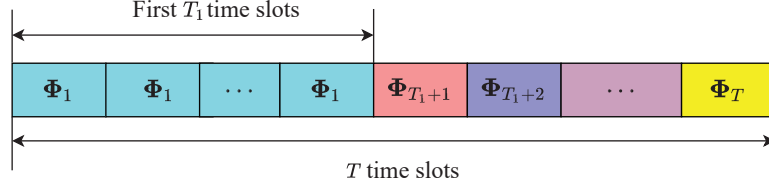


Fig. 3. Reflection matrices adopted during the training phase for the CS-EST algorithm.

slots, i.e., $\hat{\mathbf{r}} = [\mathbf{r}_1^T, \dots, \mathbf{r}_T^T]^T$ can be rewritten as $\hat{\mathbf{r}} = \Psi\boldsymbol{\mu} + \hat{\mathbf{z}}$, where $\Psi = [\Psi_1^T, \dots, \Psi_T^T]^T$ and $\hat{\mathbf{z}} = [\mathbf{z}_1^T, \dots, \mathbf{z}_T^T]^T$. Thus, the recovery of $\boldsymbol{\mu}$ is a classical sparse signal recovery problem, which can be formulated as follows

$$\begin{aligned} & \underset{\boldsymbol{\mu}}{\text{minimize}} && \|\hat{\mathbf{r}} - \Psi\boldsymbol{\mu}\|^2 \\ & \text{subject to} && \|\boldsymbol{\mu}\|_0 = PQ. \end{aligned} \quad (31)$$

CS-based algorithms, e.g., the GAMP and OMP methods, can be directly applied to recover $\boldsymbol{\mu}$, which, however, leads to a prohibitively high computational complexity of $\mathcal{O}(TG_1^2G_{\text{UE}}G_{\text{BS}}N_{\text{BS}})$ [21] and a training overhead of $\mathcal{O}(PQ\log(G_{\text{UE}}G_{\text{BS}}G_1^2))$ [20]. Therefore, in order to reduce the computational complexity, we propose to separate the overall estimation phase into three stages, where in each stage a low-complexity CS method can be applied. Specifically, in the first stage, we estimate the AoAs at the BS based on the observations in the first T_1 time slot, while the AoDs at the UE are estimated in the second stage by collecting the received pilots in all T time slots. Finally, in the third stage, we estimate the channel gains and recover the cascaded channel based on the results of the previous two stages. The proposed estimation protocol is illustrated in Fig. 3. Specifically, we set the reflection matrix Φ_t such that it is fixed as Φ_1 during the first T_1 time slots but changes in each of the other time slots, which facilitates the formulation of the estimation in each stage as a sparse signal recovery problem.

B. Estimation of the AoDs at the UE

In the first stage, we estimate the AoDs at the UE. Based on the angular domain representation in Section II-C and (1), the received pilots in the first T_1 time slots can be rewritten as follows

$$\mathbf{r}_t^H = \mathbf{s}_t^H \mathbf{H} \Phi_1^H \mathbf{G}^H + \mathbf{z}_t^H = \mathbf{s}_t^H \mathbf{A}_{\text{UE}} \underbrace{\Lambda_{\text{H}}^H \mathbf{A}_{\text{I}}^H \Phi_1^H \mathbf{G}^H}_{\Gamma_{\text{UE}}} + \mathbf{z}_t^H, \quad t \in \{1, 2, \dots, T_1\}. \quad (32)$$

Since Λ_{H} is a sparse matrix with Q non-zero elements, $\Gamma_{\text{UE}} \in \mathbb{C}^{G_{\text{UE}} \times N_{\text{BS}}}$ is a row-sparse matrix with Q non-zero rows. By collecting the pilots received in the first T_1 time slots, we have

$$\mathbf{R}_1^H = \underbrace{\mathbf{S}_1 \mathbf{A}_{\text{UE}}}_{\Theta} \Gamma_{\text{UE}} + \mathbf{Z}_1^H, \quad (33)$$

Algorithm 3 OMP Algorithm for the First Stage

- 1: Initialize $\bar{\Theta}$ and $\bar{\mathbf{A}}_{\text{UE}}$ as empty matrices, $\mathbf{R}_{\text{res}} = \mathbf{R}_1$, and $\Theta = \mathbf{S}_1 \mathbf{A}_{\text{UE}}$.
 - 2: **for** $q \leq Q$ **do**
 - 3: $\Psi = \Theta^H \mathbf{R}_{\text{res}}$;
 - 4: $k = \arg \max_{\ell} (\Psi \Psi^H)_{\ell, \ell}$;
 - 5: $\bar{\Theta} = [\bar{\Theta} \mid \Theta^{(k)}]$;
 - 6: $\bar{\mathbf{A}}_{\text{UE}} = [\bar{\mathbf{A}}_{\text{UE}} \mid \mathbf{A}_{\text{UE}}^{(k)}]$;
 - 7: $\Gamma_{\text{UE}} = (\bar{\Theta}^H \bar{\Theta})^{-1} \bar{\Theta}^H \mathbf{R}_{\text{res}}$;
 - 8: $\mathbf{R}_{\text{res}} = \mathbf{R}_1 - \bar{\Theta} \Gamma_{\text{UE}}$;
 - 9: **end for**
 - 10: Output $\bar{\mathbf{A}}_{\text{UE}}$ as the reduction of \mathbf{A}_{UE} for the third stage.
-

where $\mathbf{R}_1 = [\mathbf{r}_1, \dots, \mathbf{r}_{T_1}] \in \mathbb{C}^{N_{\text{BS}} \times T_1}$, $\mathbf{S}_1 = [\mathbf{s}_1, \dots, \mathbf{s}_{T_1}]^H \in \mathbb{C}^{T_1 \times N_{\text{UE}}}$, and $\mathbf{Z}_1 = [\mathbf{z}_1, \dots, \mathbf{z}_{T_1}] \in \mathbb{C}^{N_{\text{BS}} \times T_1}$. Notice that the i -th row of Γ_{UE} is non-zero only when the i -th column of \mathbf{A}_{UE} corresponds to one of the transmit antenna array response vectors $\mathbf{a}_{\text{UE}}(\psi_t^q)$, $q = 1, \dots, Q$, of the reflecting channel \mathbf{H} defined in (2). Thus, the estimation task in the first stage is to identify the Q columns of \mathbf{A}_{UE} corresponding to non-zero rows of Γ_{UE} based on the observation matrix \mathbf{R}_1 in (33), which is equivalent to the estimation of the AoDs at the UE. This is a sparse recovery problem that can be solved with the OMP algorithm [34]. The relevant pseudo code of the OMP algorithm is provided in **Algorithm 3**, where $\Theta^{(k)}$ and $\mathbf{A}_{\text{UE}}^{(k)}$ respectively denote the k -th column of Θ and the k -th column of \mathbf{A}_{UE} . In each iteration, we find the column of \mathbf{A}_{UE} most closely related to the updated residual. After Q iterations, an $N_{\text{UE}} \times Q$ matrix $\bar{\mathbf{A}}_{\text{UE}}$ can be constructed by extracting the Q columns of \mathbf{A}_{UE} corresponding to the non-zero rows of $\Lambda_{\mathbf{H}}^H$.

C. Estimation of the AoAs at the BS

Similarly, in the second stage, we estimate the AoAs at the BS. The received pilots in the t -th time slot can be rewritten as follows

$$\mathbf{r}_t = \mathbf{A}_{\text{BS}} \Lambda_{\mathbf{G}} \mathbf{A}_{\text{I}}^H \Phi_t \mathbf{H} \mathbf{s}_t + \mathbf{z}_t, \quad (34)$$

and then the pilots received in all T time slots can be modeled as

$$\mathbf{R} = \mathbf{A}_{\text{BS}} \underbrace{\Lambda_{\mathbf{G}} \mathbf{A}_{\text{I}}^H}_{\Gamma_{\text{BS}}} \mathbf{F} + \mathbf{Z}, \quad (35)$$

where \mathbf{R} , \mathbf{F} , and \mathbf{Z} are defined as in (14). As $\mathbf{\Gamma}_{\text{BS}} \in \mathbb{C}^{G_{\text{BS}} \times T}$ is also a row-sparse matrix, by applying the OMP algorithm, we can obtain an $N_{\text{BS}} \times P$ matrix $\bar{\mathbf{A}}_{\text{BS}}$ whose columns correspond to the non-zero rows of $\mathbf{\Lambda}_{\text{G}}$. Analogously, the P columns of $\bar{\mathbf{A}}_{\text{BS}}$ are associated with the receive antenna array response vectors $\mathbf{a}_r(\theta_r^p)$, $p = 1, \dots, P$, defined in (2), which is equivalent to the estimation of the AoAs at the BS.

D. Estimation of the Cascaded Channel

Based on the estimated $\bar{\mathbf{A}}_{\text{BS}}$ and $\bar{\mathbf{A}}_{\text{UE}}$ in the previous two stages, the angular domain representation of \mathbf{G} and \mathbf{H} can be reduced to $\mathbf{G} = \bar{\mathbf{A}}_{\text{BS}} \bar{\mathbf{\Lambda}}_{\text{G}} \mathbf{A}_{\text{I}}^H$ and $\mathbf{H} = \mathbf{A}_{\text{I}} \bar{\mathbf{\Lambda}}_{\text{H}} \bar{\mathbf{A}}_{\text{UE}}^H$, where $\bar{\mathbf{\Lambda}}_{\text{G}} \in \mathbb{C}^{P \times G_{\text{I}}}$ and $\bar{\mathbf{\Lambda}}_{\text{H}} \in \mathbb{C}^{G_{\text{I}} \times Q}$ are two submatrices obtained by eliminating all zero rows of $\mathbf{\Lambda}_{\text{G}}$ and all zero columns of $\mathbf{\Lambda}_{\text{H}}$, respectively. The expression for \mathbf{r}_t can then be rewritten as follows

$$\begin{aligned} \mathbf{r}_t &= \bar{\mathbf{A}}_{\text{BS}} \bar{\mathbf{\Lambda}}_{\text{G}} \mathbf{A}_{\text{I}}^H \Phi_t \mathbf{A}_{\text{I}} \bar{\mathbf{\Lambda}}_{\text{H}} \bar{\mathbf{A}}_{\text{UE}}^H \mathbf{s}_t + \mathbf{z}_t \\ &= ((\mathbf{s}_t^T \bar{\mathbf{A}}_{\text{UE}}^*) \otimes \bar{\mathbf{A}}_{\text{BS}}) (\bar{\mathbf{\Lambda}}_{\text{H}}^T \otimes \bar{\mathbf{\Lambda}}_{\text{G}}) (\mathbf{A}_{\text{I}}^T \odot \mathbf{A}_{\text{I}}^H) \mathbf{v}_t + \mathbf{z}_t, \end{aligned} \quad (36)$$

where we used $(\mathbf{A}\mathbf{B}) \odot (\mathbf{C}\mathbf{D}) = (\mathbf{A} \otimes \mathbf{C}) (\mathbf{B} \odot \mathbf{D})$. Based on the formulation of the overcomplete matrices in (8), we have that $\mathbf{A}_{\text{I}}^T \odot (\mathbf{a}_j^H \otimes \mathbf{1}_{G_{\text{I}}}) = \mathbf{L}_j \mathbf{A}_{\text{I}}^T$, where $\mathbf{a}_j \in \mathbb{C}^M$ denotes the j -th column of \mathbf{A}_{I} and $\mathbf{L}_j \in \mathbb{C}^{G_{\text{I}} \times G_{\text{I}}}$ is a permutation matrix that rearranges the rows of \mathbf{A}_{I} [35]. Therefore, the term $(\bar{\mathbf{\Lambda}}_{\text{H}}^T \otimes \bar{\mathbf{\Lambda}}_{\text{G}}) (\mathbf{A}_{\text{I}}^T \odot \mathbf{A}_{\text{I}}^H)$ in (36) can be simplified as follows

$$\begin{aligned} (\bar{\mathbf{\Lambda}}_{\text{H}}^T \otimes \bar{\mathbf{\Lambda}}_{\text{G}}) (\mathbf{A}_{\text{I}}^T \odot \mathbf{A}_{\text{I}}^H) &= \begin{bmatrix} \bar{\lambda}_1 \otimes \bar{\mathbf{\Lambda}}_{\text{G}} & \dots & \bar{\lambda}_{G_{\text{I}}} \otimes \bar{\mathbf{\Lambda}}_{\text{G}} \end{bmatrix} \begin{bmatrix} \mathbf{L}_1 \mathbf{A}_{\text{I}}^T \\ \vdots \\ \mathbf{L}_{G_{\text{I}}} \mathbf{A}_{\text{I}}^T \end{bmatrix} \\ &= \underbrace{\left(\sum_{j=1}^{G_{\text{I}}} (\bar{\lambda}_j \otimes \bar{\mathbf{\Lambda}}_{\text{G}}) \mathbf{L}_j \right)}_{\hat{\mathbf{\Lambda}}} \mathbf{A}_{\text{I}}^T, \end{aligned} \quad (37)$$

where $\bar{\lambda}_j \in \mathbb{C}^Q$ denotes the j -th column of $\bar{\mathbf{\Lambda}}_{\text{H}}^T$ and $\hat{\mathbf{\Lambda}} \in \mathbb{C}^{PQ \times G_{\text{I}}}$ is a sparse matrix with PQ non-zero elements. Finally, by substituting the result of (37) into (36), we have

$$\mathbf{r}_t = ((\mathbf{s}_t^T \bar{\mathbf{A}}_{\text{UE}}^*) \otimes \bar{\mathbf{A}}_{\text{BS}}) \hat{\mathbf{\Lambda}} \mathbf{A}_{\text{I}}^T \mathbf{v}_t + \mathbf{z}_t = ((\mathbf{v}_t^T \mathbf{A}_{\text{I}}) \otimes (\mathbf{s}_t^T \bar{\mathbf{A}}_{\text{UE}}^*) \otimes \bar{\mathbf{A}}_{\text{BS}}) \boldsymbol{\lambda} + \mathbf{z}_t,$$

where $\boldsymbol{\lambda} = \text{vec}(\hat{\mathbf{\Lambda}}) \in \mathbb{C}^{PQG_{\text{I}}}$ is a sparse vector with PQ non-zero elements. Subsequently, all pilots received over all T time slots can be collected in vector

$$\hat{\mathbf{r}} = \begin{bmatrix} (\mathbf{v}_1^T \mathbf{A}_{\text{I}}) \otimes (\mathbf{s}_1^T \bar{\mathbf{A}}_{\text{UE}}^*) \otimes \bar{\mathbf{A}}_{\text{BS}} \\ \vdots \\ (\mathbf{v}_T^T \mathbf{A}_{\text{I}}) \otimes (\mathbf{s}_T^T \bar{\mathbf{A}}_{\text{UE}}^*) \otimes \bar{\mathbf{A}}_{\text{BS}} \end{bmatrix} \boldsymbol{\lambda} + \hat{\mathbf{z}}. \quad (38)$$

For the sake of complexity reduction, we adopt the OMP algorithm to recover the sparse vector λ . Finally, with the obtained λ , the cascaded channel $\mathbf{H}_c \triangleq \mathbf{H}^T \odot \mathbf{G}$ can be recovered as follows

$$\mathbf{H}_c = (\bar{\mathbf{A}}_{\text{UE}}^* \bar{\mathbf{A}}_{\text{H}}^T \mathbf{A}_{\text{I}}^T) \odot (\bar{\mathbf{A}}_{\text{BS}} \bar{\mathbf{A}}_{\text{G}} \mathbf{A}_{\text{I}}^H) = (\bar{\mathbf{A}}_{\text{UE}}^* \otimes \bar{\mathbf{A}}_{\text{BS}}) \bar{\mathbf{A}} \mathbf{A}_{\text{I}}^T, \quad (39)$$

where $\bar{\mathbf{A}}$ is obtained by reshaping λ to a $PQ \times G_{\text{I}}$ matrix and the proposed estimation scheme is referred to as the **CS-EST algorithm**. Although the proposed approach cannot separately estimate the individual channel matrices, i.e., \mathbf{G} and \mathbf{H} , in the next section, we will illustrate that knowledge of the cascaded channel matrix \mathbf{H}_c is sufficient for system design after the channel estimation phase, e.g., for downlink beamforming design. The computational complexities of the three stages of the proposed CE-EST algorithm are $\mathcal{O}(QT_1 N_{\text{UE}} G_{\text{UE}})$, $\mathcal{O}(PT N_{\text{BS}} G_{\text{BS}})$, and $\mathcal{O}(P^2 Q^2 T G_{\text{I}} N_{\text{BS}})$, respectively, which is significantly lower compared with that for directly solving problem (35) and that of the MO-EST algorithm proposed in Section III. On the other hand, note that recovering an $n \times 1$ vector with m non-zero elements requires the dimension of the observation to be on the order of $\mathcal{O}(m \log(mn))$ [20], [35]. Therefore, the required training overhead of the proposed CS-EST algorithm is given by $T \geq \mathcal{O}(Q \log(Q G_{\text{UE}}) + PQ \log(PQ G_{\text{I}}))$, which is typically much smaller than that of simple LS estimation, i.e., $T \geq MN_{\text{UE}}$, without consideration of the unique properties of mm-wave channels. The training overhead reduction shall also be verified via simulation in Section VI.

V. ALT-WMMSE ALGORITHM

In this section, we propose a downlink beamforming design based on the knowledge of the cascaded channel matrix, \mathbf{H}_c , obtained with the channel estimation schemes proposed in Sections III and IV.

A. Problem Formulation

By utilizing the reciprocity of the uplink and downlink channels, the estimated uplink channel matrix can be utilized for downlink data transmission in the IRS-assisted system considered in Section II. Assuming that the BS aims to transmit N_s data streams to the UE, the received signal $\mathbf{y} \in \mathbb{C}^{N_{\text{UE}}}$ can be written as follows

$$\mathbf{y} = \mathbf{H}^H \Phi_{\text{d}} \mathbf{G}^H \mathbf{F} \mathbf{x} + \mathbf{z}_{\text{d}}, \quad (40)$$

where $\mathbf{F} \in \mathbb{C}^{N_{\text{BS}} \times N_s}$ represents the beamformer at the BS and $\mathbf{x} \in \mathbb{C}^{N_s}$ denotes the symbol vector with $\mathbb{E}\{\mathbf{x}\mathbf{x}^H\} = \mathbf{I}_{N_s}$ without loss of generality. $\Phi_{\text{d}} = \text{diag}(\mathbf{v}_{\text{d}})$ denotes the downlink reflection

matrix and $\mathbf{z}_d \in \mathbb{C}^{N_{\text{UE}}}$ denotes the downlink additive Gaussian noise with $\mathbf{z}_d \sim \mathcal{CN}(\mathbf{0}, \sigma_d^2 \mathbf{I}_{N_{\text{UE}}})$. By exploiting a property of the Khatri-Rao product, we have

$$\mathbf{H}^H \Phi_d \mathbf{G}^H = \text{mat}((\mathbf{G}^* \odot \mathbf{H}^H) \mathbf{v}_d) = \text{mat}(\mathbf{K} \mathbf{H}_c^* \mathbf{v}_d) \triangleq \mathbf{H}_e, \quad (41)$$

where $\text{mat}(\cdot)$ denotes the operation that reshapes an $N_{\text{BS}} N_{\text{UE}} \times 1$ vector to an $N_{\text{UE}} \times N_{\text{BS}}$ matrix. $\mathbf{K} \in \mathbb{C}^{N_{\text{BS}} N_{\text{UE}} \times N_{\text{BS}} N_{\text{UE}}}$ denotes the commutation matrix, which is a constant matrix for given N_{BS} and N_{UE} [35]. \mathbf{H}_e is defined as the effective channel matrix, based on which (40) can be further rewritten as $\mathbf{y} = \mathbf{H}_e \mathbf{F} \mathbf{x} + \mathbf{z}_d$. Then, the achievable spectral efficiency when the transmitted symbols follow a complex Gaussian distribution can be expressed as follows

$$R = \left(1 - \frac{T}{T_{\text{tot}}}\right) \log \left| \mathbf{I}_{N_s} + \frac{1}{\sigma_d^2} \mathbf{F}^H \mathbf{H}_e^H \mathbf{H}_e \mathbf{F} \right|, \quad (42)$$

where T_{tot} denotes the total number of time slots within the channel coherence time. In this section, our goal is to maximize the spectral efficiency by optimizing the beamformer at the BS and the reflection matrix at the IRS.

Remark 2: From (42) and (43), we observe that the CSI of the effective channel, \mathbf{H}_e , is sufficient for the design of the downlink beamformer and the reflection matrix. With the MO-EST algorithm, we obtain the CSI for \mathbf{H} and \mathbf{G} separately. Hence, \mathbf{H}_e can be directly composed according to (41). On the other hand, with the CS-EST algorithm, the cascaded channel, \mathbf{H}_c , is estimated via (39), and therefore, \mathbf{H}_e can be formed according to (41). In the following, we show how to design the beamformer and the IRS reflection matrix for downlink data transmission based on \mathbf{H}_e , or, in other words, the CSI estimated by the two proposed algorithms.

To this end, we resort to the equivalent WMMSE minimization problem [36, eq. (32)]

$$\begin{aligned} & \underset{\mathbf{F}, \mathbf{W}, \mathbf{v}_d, \Omega}{\text{minimize}} && g = \text{tr}(\Omega \mathbf{E}) - \log |\Omega| \\ & \text{subject to} && \|\mathbf{F}\|_F^2 \leq 1, \quad |[\mathbf{v}_d]_n| = 1 \quad \forall n, \end{aligned} \quad (43)$$

where $\|\mathbf{F}\|_F^2 \leq 1$ denotes the normalized transmit power constraint and $|[\mathbf{v}_d]_n| = 1$ is the constant modulus constraint imposed by the phase shifters. Furthermore, $\mathbf{E} \in \mathbb{C}^{N_s \times N_s}$ is the MSE matrix, which is given by [37]

$$\mathbf{E} = \mathbb{E} \left[(\mathbf{x} - \mathbf{y}) (\mathbf{x} - \mathbf{y})^H \right] = \mathbf{I}_{N_s} - \mathbf{F}^H \mathbf{H}_e^H \mathbf{W} - \mathbf{W}^H \mathbf{H}_e \mathbf{F} + \sigma_d^2 \mathbf{W}^H \mathbf{W} + \mathbf{W}^H \mathbf{H}_e \mathbf{F} \mathbf{F}^H \mathbf{H}_e^H \mathbf{W},$$

with $\Omega \in \mathbb{C}^{N_s \times N_s}$ and $\mathbf{W} \in \mathbb{C}^{N_{\text{UE}} \times N_s}$ being two auxiliary variables. By applying the AM principle, in the following, we alternately optimize these variables.

B. Optimization of the Beamformer

Aiming at problem (43), when fixing \mathbf{F} and \mathbf{v}_d , closed-form solutions for \mathbf{W} and Ω are given by

$$\mathbf{W} = (\mathbf{H}_e \mathbf{F} \mathbf{F}^H \mathbf{H}_e^H + \sigma_d^2 \mathbf{I}_{N_{UE}})^{-1} \mathbf{H}_e \mathbf{F}, \quad \Omega = \mathbf{E}^{-1}. \quad (44)$$

Similarly, when \mathbf{v}_d , \mathbf{W} , and Ω are fixed, a closed-form solution of \mathbf{F} is given by

$$\mathbf{F} = \xi \tilde{\mathbf{F}}, \quad \xi = \left(\text{tr} \left(\tilde{\mathbf{F}} \tilde{\mathbf{F}}^H \right) \right)^{-\frac{1}{2}}, \quad (45)$$

where $\tilde{\mathbf{F}} = (\mathbf{H}_e^H \mathbf{W} \Omega \mathbf{W}^H \mathbf{H}_e + \sigma^2 \psi \mathbf{I}_{N_{BS}})^{-1} \mathbf{H}_e^H \mathbf{W} \Omega$ denotes the unnormalized baseband beamformer and $\psi \triangleq \text{tr}(\Omega \mathbf{W}^H \mathbf{W})$. Hence, recalling the definition of \mathbf{H}_e in (41), the CSI of \mathbf{H}_c is sufficient to obtain closed-form solutions.

C. Optimization of the Reflection Matrix

In this subsection, we focus on the optimization of g in (43) with respect to \mathbf{v}_d by fixing the other variables. The corresponding subproblem is given by

$$\begin{aligned} & \underset{\mathbf{v}_d}{\text{minimize}} \quad g_1(\mathbf{v}_d) = \text{tr}(-\Omega \mathbf{F}^H \mathbf{H}_e^H \mathbf{W} - \Omega \mathbf{W}^H \mathbf{H}_e \mathbf{F} + \Omega \mathbf{W}^H \mathbf{H}_e \mathbf{F} \mathbf{F}^H \mathbf{H}_e^H \mathbf{W}) \\ & \text{subject to} \quad |[\mathbf{v}_d]_n| = 1 \quad \forall n. \end{aligned} \quad (46)$$

Instead of directly solving problem (46), we further substitute the closed-form solution of \mathbf{W} given by (44) into $g_1(\mathbf{v}_d)$, which yields

$$g_1(\mathbf{v}_d) = \text{tr} \left(\left(\Omega^{-1} + \frac{1}{\sigma_d^2} \Omega^{-1} \mathbf{F}^H \mathbf{H}_e^H \mathbf{H}_e \mathbf{F} \right)^{-1} \right). \quad (47)$$

The feasible set of \mathbf{v}_d is also a well-known complex circle Riemannian manifold [28], [37], i.e., $\mathcal{M} \triangleq \{\mathbf{x} \in \mathbb{C}^M : |[\mathbf{x}]_n| = 1, \forall n\}$. Therefore, the MO technique can be applied to optimize \mathbf{v}_d . Based on basic differentiation rules for complex-valued matrices [38], the differential is given by

$$d(g_1) \stackrel{(b)}{=} -\frac{1}{\sigma_d^2} \text{tr} \left(\mathbf{T}^{-2} \Omega^{-1} \mathbf{F}^H d(\mathbf{H}_e^H) \mathbf{H}_e \mathbf{F} \right) \stackrel{(c)}{=} -\frac{1}{\sigma_d^2} \mathbf{m}^T d(\mathbf{H}_e^H) \stackrel{(d)}{=} -\frac{1}{\sigma_d^2} \mathbf{m}^T \mathbf{H}_c d(\mathbf{v}_d^*), \quad (48)$$

where $\mathbf{T} \triangleq \Omega^{-1} + \frac{1}{\sigma_d^2} \Omega^{-1} \mathbf{F}^H \mathbf{H}_e^H \mathbf{H}_e \mathbf{F}$ and $\mathbf{m} \triangleq \text{vec} \left((\mathbf{H}_e \mathbf{F} \mathbf{T}^{-2} \Omega^{-1} \mathbf{F}^H)^T \right)$ are defined for notational brevity. Note that (b) follows from $d(\mathbf{X}^{-1}) = -\mathbf{X}^{-1} d(\mathbf{X}^{-1}) \mathbf{X}^{-1}$, (c) follows from $\text{tr}(\mathbf{A} \mathbf{B}) = (\text{vec}(\mathbf{A}^T))^T \text{vec}(\mathbf{B})$, and (d) follows from $\text{vec}(\mathbf{H}_e^H) = (\mathbf{H}^T \odot \mathbf{G}) \mathbf{v}_d^*$. Based on (48) and using $d(g_1) = (\nabla_{\mathbf{v}_d^*} g_1)^T d(\mathbf{v}_d^*)$, the gradient of g_1 with respect to \mathbf{v}_d^* is given by

$$\nabla_{\mathbf{v}_d^*} g_1 = -\frac{1}{\sigma_d^2} \mathbf{H}_c^T \mathbf{m}. \quad (49)$$

Algorithm 4 ALT-WMMSE Algorithm

- 1: Set $i = 0$, randomly initialize $\mathbf{v}_d^{(0)}$ and $\mathbf{F}^{(0)}$.
 - 2: Solve $\mathbf{W}^{(0)}$ and $\mathbf{\Omega}^{(0)}$ according to (44) and set $g^{(0)} = g(\mathbf{W}^{(0)}, \mathbf{F}^{(0)}, \mathbf{\Omega}^{(0)}, \mathbf{v}_d^{(0)})$;
 - 3: **repeat**
 - 4: Update $\mathbf{v}_d^{(i+1)}$ via MO optimization with the Euclidean gradient derived in (49);
 - 5: Update $\mathbf{W}^{(i+1)}$ and $\mathbf{\Omega}^{(i+1)}$ with the closed-form solutions in (44);
 - 6: Update $\mathbf{F}^{(i+1)}$ with the closed-form solutions in (45);
 - 7: $i \leftarrow i + 1$;
 - 8: $g^{(i)} = g(\mathbf{W}^{(i)}, \mathbf{F}^{(i)}, \mathbf{\Omega}^{(i)}, \mathbf{v}_d^{(i)})$;
 - 9: **until** $g^{(i-1)} - g^{(i)} \leq \epsilon_3$.
-

Given the derived conjugate Euclidean gradient, MO can be straightforwardly applied to optimize \mathbf{v}_d under the constant modulus constraint [28]. From (48) and (49) we observe that knowledge of \mathbf{H}_c is also sufficient for the optimization of \mathbf{v}_d .

D. ALT-WMMSE Algorithm

Based on the previous subsections, the joint optimization of the beamformer and the reflection matrix can be accomplished by alternately optimizing the variables. The overall ALT-WMMSE algorithm is summarized in **Algorithm 4**, where ϵ_3 is the convergence threshold. Notice that since in each step the variables are updated based on closed-form solutions or monotonous descent algorithms [31], the ALT-WMMSE algorithm is guaranteed to converge to a stationary point of problem (43) [31]. The computational complexity of the proposed algorithm is $\mathcal{O}(N_{\text{BS}}N_{\text{UE}}M)$, which is mainly caused by the computation of the Euclidean gradient.

VI. SIMULATION RESULTS

A. Simulation Setup

According to the channel model in (2), without loss of generality, we denote $p = 1$ and $q = 1$ as the indices of the LoS components in \mathbf{G} and \mathbf{H} , respectively. If not specified otherwise, for both \mathbf{H} and \mathbf{G} , the same number of paths is assumed, i.e., $P = Q \triangleq K = 3$. The complex channel gains of the LoS components are distributed as $\alpha_1 \sim \mathcal{CN}(0, \tau_{\text{BI}})$ and $\beta_1 \sim \mathcal{CN}(0, \tau_{\text{IU}})$, while those of the NLoS components are distributed as $\alpha_i \sim \mathcal{CN}(0, 10^{-0.5}\tau_{\text{BI}})$ and $\beta_i \sim \mathcal{CN}(0, 10^{-0.5}\tau_{\text{IU}})$ for $i = 2, \dots, K$ [39], [40], where τ_{BI} and τ_{IU} are given by [23]

$$\tau_{\text{BI}} = 10^{-6.14-2\log_{10}(d_{\text{BI}})} \quad \text{and} \quad \tau_{\text{IU}} = 10^{-6.14-2\log_{10}(d_{\text{IU}})}. \quad (50)$$

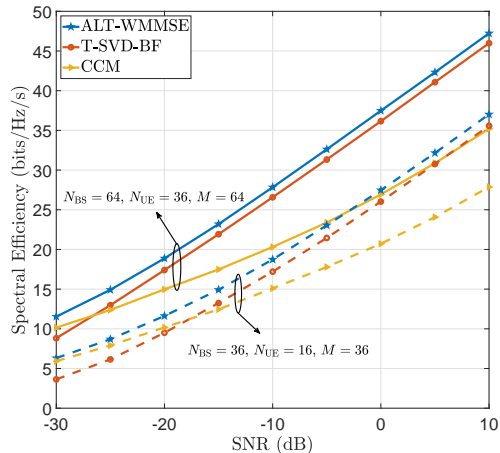


Fig. 4. Spectral efficiency versus SNR for different beamforming algorithms in IRS-assisted mm-wave MIMO systems.

Here, d_{BI} represents the distance between the BS and the IRS and is set to 150 m, while d_{IU} denotes the distance between the IRS and the UE and is set to 10 m. The azimuth and elevation AoAs/AoDs are generated uniformly distributed in $(0, 2\pi]$. T_{tot} is set to 2000, corresponding to a channel coherence time of 5 ms for a transmission bandwidth of 4×10^5 Hz. The convergence thresholds ϵ_1 , ϵ_2 , and ϵ_3 are all set to 10^{-3} . The uplink training pilot-to-noise-ratio (PNR) is defined as $\frac{P_{\text{tr}}\tau_{\text{BI}}\tau_{\text{IU}}}{\sigma_d^2}$, while the downlink transmission signal-to-noise-ratio (SNR) is defined as $\frac{\tau_{\text{BI}}\tau_{\text{IU}}}{\sigma_d^2}$. All simulation results are averaged over 1000 independent channel realizations.

B. Performance of the ALT-WMMSE Algorithm

In this subsection, to show the effectiveness of the proposed ALT-WMMSE beamforming algorithm, we first evaluate its performance in terms of spectral efficiency (42) assuming perfect knowledge of \mathbf{H} and \mathbf{G} with $T = 0$. Two state-of-the-art passive beamforming algorithms are adopted as benchmarks, namely, the complex circle manifold (CCM) algorithm [22] and the truncated-SVD-based beamforming (T-SVD-BF) algorithm [23]. The CCM algorithm optimizes \mathbf{v}_d by minimizing the objective of problem (46) without substituting the optimal solution (44) into (46). On the other hand, the T-SVD-BF algorithm assumes equal power allocation among different data streams to simplify the problem. Fig. 4 shows the spectral efficiency as a function of the SNR for two different system configurations when $N_s = 3$. As can be observed, the proposed ALT-WMMSE algorithm achieves the highest spectral efficiency over the entire SNR range considered. This shows the superiority of the proposed ALT-WMMSE beamforming algorithm for rate maximization. In particular, as the optimal solution of \mathbf{W} is used for solving problem (46), the spectral efficiency achieved by the ALT-WMMSE algorithm is significantly

TABLE I
NUMBER OF FLOPS REQUIRED FOR THE CS-EST AND GAMP ALGORITHMS WITH RESPECT TO F .

Angular resolution F	8	16	32	64	128
Algorithm					
CS-EST	9.35×10^6	1.87×10^7	3.74×10^7	7.48×10^7	1.5×10^8
GAMP	4.72×10^9	7.54×10^{10}	1.21×10^{12}	1.93×10^{13}	3.09×10^{14}

improved compared to the CCM algorithm. Furthermore, since equal power allocation is only asymptotically optimal in the high SNR regime, the performance of the T-SVD-BF algorithm entails a significant loss for low SNRs. Therefore, in the remainder of this section, the ALT-WMMSE algorithm is adopted for beamforming to evaluate the downlink spectral efficiency with imperfect knowledge of \mathbf{H}_c , which is obtained with different channel estimation schemes.

C. Benchmark Schemes

In this section, the PARAFAC algorithm [18], [19] and the GAMP algorithm [20] are adopted as two state-of-the-art benchmark schemes. The PARAFAC algorithm models the received pilots as a tensor and then obtains the channel matrices based on the LS criterion without exploiting the low-rank and sparse properties of mm-wave channels revealed in Lemmas 1 and 2. The GAMP algorithm treats the channel estimation problem as a classical sparse signal recovery problem (31). During the channel training phase, for all considered algorithms, we adopt random quasi-omnidirectional training beams [26], i.e., the entries of \mathbf{v}_t and \mathbf{s}_t , $t = 1, \dots, T$, are randomly chosen on the complex unit circle, and set $N_{\text{BS}} = 36$, $N_{\text{UE}} = 16$, and $M = 36$. To facilitate a fair comparison between the CS-EST and GAMP algorithms, we list the number of required floating point operations (FLOPs) with respect to the angular resolution, F , for both algorithms in Table I when $T = 100$. In particular, the angular resolutions at the BS and the UE are set to $G_{\text{BS}} = G_{\text{UE}} = F$. Since the IRS is typically considered to be a large-scale planar array, a higher resolution is assumed at the IRS, i.e., $G_{\text{I}} = 4F$, to achieve a satisfactory estimation performance.

Consistent with the complexity analysis in Sections III and IV, Table I shows that the required numbers of FLOPs for the CS-EST and GAMP algorithms scales with F and F^4 , respectively. Thus, in the remainder of this section, for the proposed CS-EST algorithm, we adopt $F = 64$, i.e., $G_{\text{BS}} = 64$, $G_{\text{UE}} = 64$, and $G_{\text{I}} = 256$ (16×16). In contrast, in order to achieve an affordable complexity, for the GAMP algorithm F is reduced to $F = 16$, i.e., $G_{\text{BS}} = 16$, $G_{\text{UE}} = 16$, and $G_{\text{I}} = 64$ (8×8). Note that the computational complexity of the proposed CS-EST algorithm is

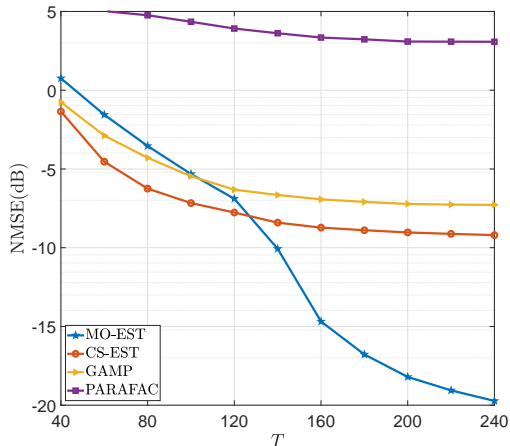


Fig. 5. NMSE versus T for different channel estimation algorithms when PNR = 0 dB.

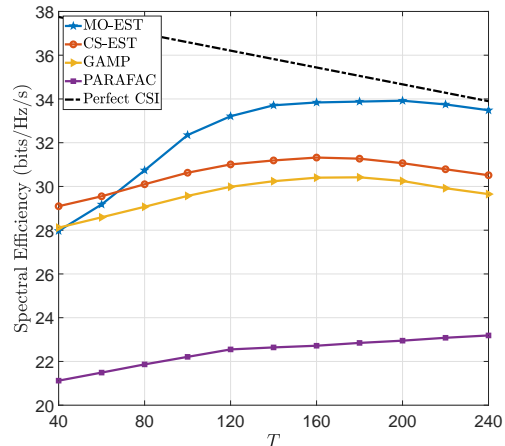


Fig. 6. Spectral efficiency versus T for different channel estimation algorithms when PNR = SNR = 10 dB.

still much lower than that of the GAMP algorithm even though a higher angular resolution is adopted for the CS-EST algorithm.

D. System Performance Versus Training Overhead

Now, we evaluate the performance of the two proposed channel estimation algorithms. In Fig. 5, we plot the normalized mean square error (NMSE) versus the training overhead, T , for PNR = 0 dB. The NMSE is defined as $\mathbb{E} \left\{ \|\mathbf{H}_c - \hat{\mathbf{H}}_c\|_F^2 / \|\mathbf{H}_c\|_F^2 \right\}$. As can be observed, the NMSE of all algorithms decreases with increasing training overhead T . Since the PARAFAC algorithm requires a training overhead of $T \geq MN_{\text{UE}}$ [18], it is not well suited for the considered range of T and results in the worst performance. In contrast, thanks to the fixed-rank constraints and ℓ_1 -norm regularization, MO is able to find a sparse solution in the angular domain and therefore achieves a lower NMSE with much fewer pilots. Besides, although the MO-EST algorithm suffers from a performance loss for small T , its performance improves rapidly as T increases and it achieves the lowest NMSE among all investigated algorithms for $T \geq 130$. On the other hand, as shown in Section IV, the number of time slots required for the CS-EST algorithm is only in the order of $\mathcal{O}(Q \log(QG_{\text{UE}}) + PQ \log(PQG_{\text{I}}))$. Consequently, the CS-EST algorithm achieves the lowest NMSE for small T . Meanwhile, it outperforms the GAMP algorithm as it can afford a higher angular resolution, i.e., larger G_{BS} , G_{UE} , and G_{I} , because of its lower computational complexity according to Table I. However, the finite angular resolution becomes the main bottleneck for further improving of the performance for large T , which causes the NMSEs of both the CS-EST and the GAMP algorithms to saturate.

TABLE II
NUMBER OF REQUIRED FLOPs FOR ALL SIMULATED ALGORITHMS.

Algorithm	CS-EST	GAMP	MO-EST	PARAFAC
FLOPs	1.50×10^8	1.51×10^{11}	8.52×10^8	3.54×10^8

In Fig. 6, we plot the spectral efficiency versus the training overhead, T . For beamforming, the ALT-WMMSE algorithm is applied, where the effective channel estimate $\hat{\mathbf{H}}_e$ obtained by different algorithms is adopted. We set downlink SNR = 10 dB, $N_s = 3$, and PNR = 10 dB. As can be observed from Fig. 6, the spectral efficiency of all algorithms increases with T when $T \leq 160$, thanks to the improved accuracy of the CSI. If T is increased further (e.g., $T \geq 200$), for the GAMP, CS-EST, and MO-EST algorithms, the larger T cannot significantly improve the CSI further, and thus, the corresponding spectral efficiencies decrease due to the increasing training overhead. The MO-EST algorithm achieves the best performance when $T \geq 70$ and gradually approaches the performance upper bound achieved with perfect CSI². Hence, Figs. 5 and 6 both suggest that the MO-EST algorithm can be regarded as a performance benchmark for sufficiently large T , while the CS-EST algorithm achieves high performance, especially when the budget for training overhead is limited.

E. System Performance Versus PNR

Next, in Figs. 7 and 8, we show the NMSE and the spectral efficiency versus the PNR, respectively. For the MO-EST, CS-EST, and GAMP algorithms, the training overhead T is set to 200. On the other hand, we set T to the minimum required value of $T = MN_t = 576$ for the PARAFAC algorithm [18]. Nevertheless, as can be observed, there is a large performance gap between the PARAFAC and the MO-EST algorithms. This is mainly because the proposed MO-EST algorithm efficiently exploits the sparsity of mm-wave channels, which highlights the importance of incorporating the rank constraints and ℓ_1 -norm regularizations into the channel estimation algorithm design for IRS-assisted mm-wave MIMO systems. Meanwhile, it can be seen that for the CS-EST and GAMP algorithms, the performance gains achieved by increasing the PNR are relatively small. This is because the main bottleneck in the high PNR regime is the adopted limited angular resolutions. Furthermore, for the parameter settings of Figs. 7 and

²For a fair comparison, we assume that the training overhead of this upper bound benchmark scheme is the same as for the estimated CSI case.

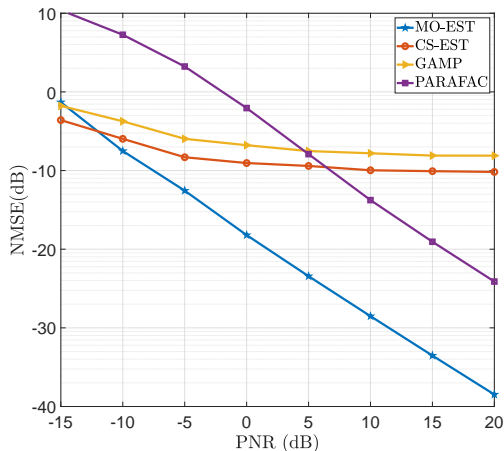


Fig. 7. NMSE versus PNR for different channel estimation algorithms.

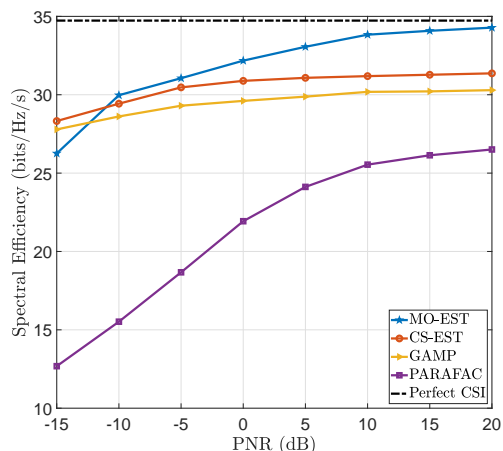


Fig. 8. Spectral efficiency versus PNR for different channel estimation algorithms when SNR = 10 dB.

8, we list the computational complexity of all investigated algorithms in Table II. The results in Table II, Fig. 7, and Fig. 8 clearly illustrate the superiority of the proposed MO-EST algorithm especially for channel estimation with high PNRs, which comes at the expense of a higher computational complexity compared to the CS-EST algorithm. On the other hand, the CS-EST algorithm achieves an excellent trade-off between estimation performance and computational complexity.

F. Robustness of the Proposed Channel Estimation Algorithms

Finally, in Fig. 9, we consider the case where the number of paths, K , is not perfectly known for channel estimation and test the robustness of the MO-EST and CS-EST algorithms with respect to the resulting uncertainty, when PNR = SNR = 10 dB and $T = 200$. As can be observed, the proposed MO-EST and CS-EST algorithms achieve the highest spectral efficiency when $\hat{K} = K$, i.e., the number of paths is perfectly known. On the other hand, a mismatch between the estimated \hat{K} and the true value of K leads to a performance loss, which, nevertheless, is limited especially when $\hat{K} \geq K$. In particular, for the MO-EST algorithm, the channel matrix \mathbf{H}_c and its estimate $\hat{\mathbf{H}}_c$ can be decomposed via SVD, i.e., $\mathbf{H}_c = \sum_{k=1}^K \zeta_k \mathbf{u}_k \mathbf{q}_k^H$ and $\hat{\mathbf{H}}_c = \sum_{k=1}^{\hat{K}} \hat{\zeta}_k \hat{\mathbf{u}}_k \hat{\mathbf{q}}_k^H$, where ζ_k ($\hat{\zeta}_k$), \mathbf{u}_k ($\hat{\mathbf{u}}_k$), and \mathbf{q}_k ($\hat{\mathbf{q}}_k$) denote the ordered singular values, left singular vectors, and right singular vectors, respectively. In order to minimize the objective function in (13) based on the LS criterion, the MO-EST algorithm tries to choose the K largest singular values of $\hat{\mathbf{H}}_c$ and the corresponding singular vectors close to the true values while keeping the remaining $\hat{K} - K$ singular values small. In other words, the solution obtained by

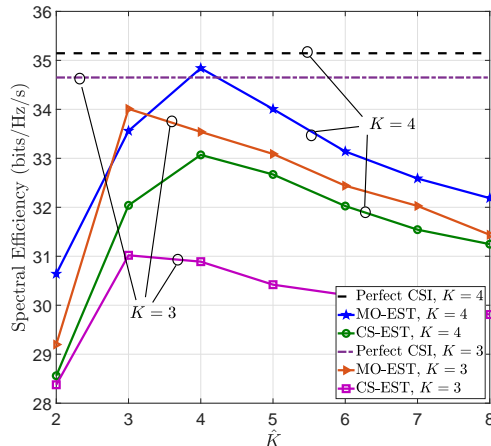


Fig. 9. Spectral efficiency versus \hat{K} for the proposed estimation algorithms when $N_s = 3$.

the MO-EST algorithm satisfies $\hat{\zeta}_k \approx \zeta_k$, $\hat{\mathbf{u}}_k \approx \mathbf{u}_k$, $\hat{\mathbf{q}}_k \approx \mathbf{q}_k$ for $k = 1, \dots, K$, and $\hat{\zeta}_k \approx 0$ for $k = K + 1, \dots, \hat{K}$, which leads to a satisfactory estimation performance when $\hat{K} \geq K$. Hence, the proposed MO-EST algorithm is robust with respect to imperfect knowledge of the exact numbers of paths of the estimated channels. Furthermore, for the CS-EST algorithm, since the OMP method itself selects the K columns most relevant to the residual, the principle components of the channel are not omitted when $\hat{K} \geq K$, and thus, the performance loss is also limited.

VII. CONCLUSIONS

In this paper, we investigated the channel estimation problem for IRS-assisted mm-wave MIMO systems. By exploiting the sparsity of the mm-wave channel, an MO-based alternating optimization algorithm and a CS-based algorithm, i.e., the MO-EST algorithm and the CS-EST algorithm, were developed to effectively estimate the IRS-assisted channels. Meanwhile, exploiting the channel estimates, we also proposed a novel downlink passive beamforming algorithm for maximization of the spectral efficiency by solving an equivalent WMMSE problem. Simulation results showed the performance improvements achieved with the proposed estimation and beamforming algorithms compared to several state-of-the-art benchmark schemes. For high PNRs and sufficient number of pilots, the MO-EST algorithm achieves the best performance. On the other hand, the CS-EST algorithm strikes a good balance between the achievable performance, computational complexity, and training overhead. Furthermore, both proposed algorithms are robust against imperfect knowledge of the sparsity level of the channels. Extending the proposed schemes to multi-user and broadband scenarios are interesting directions for future research.

APPENDIX A

We first prove that $\text{rank}(\mathbf{G}) = P$. As all AoDs of the IRS-BS channel are different, matrices $\mathbf{A}_y = [\mathbf{a}_y(\theta_t^1, \phi_t^1), \dots, \mathbf{a}_y(\theta_t^P, \phi_t^P)] \in \mathbb{C}^{M_y \times P}$ and $\mathbf{A}_z = [\mathbf{a}_z(\phi_t^1), \dots, \mathbf{a}_z(\phi_t^P)] \in \mathbb{C}^{M_z \times P}$ are both Vandermonde matrices, whose column vectors are linearly independent. Therefore, matrix $\mathbf{A}_t = [\mathbf{a}_t(\theta_t^1, \phi_t^1), \dots, \mathbf{a}_t(\theta_t^P, \phi_t^P)] \in \mathbb{C}^{M \times P}$ with linearly independent columns $\mathbf{a}_t(\theta_t^p, \phi_t^p) = \mathbf{a}_y(\theta_t^p, \phi_t^p) \otimes \mathbf{a}_z(\phi_t^p)$, for $p = 1, \dots, P$, satisfies that $\text{rank}(\mathbf{A}_t) = P$. Similarly, $\mathbf{A}_r = [\mathbf{a}_r(\theta_r^1), \dots, \mathbf{a}_r(\theta_r^P)] \in \mathbb{C}^{N_{\text{BS}} \times P}$ also satisfies $\text{rank}(\mathbf{A}_r) = P$. According to (2), \mathbf{G} can be expressed as

$$\mathbf{G} = \mathbf{A}_r \mathbf{\Sigma} \mathbf{A}_t^H, \quad (51)$$

where $\mathbf{\Sigma} = \text{diag}(\alpha^1, \dots, \alpha^P)$ is also a rank- P matrix. According to the rank properties of matrices [35], we have

$$\text{rank}(\mathbf{A}\mathbf{B}) \geq \text{rank}(\mathbf{A}) + \text{rank}(\mathbf{B}) - k, \quad \text{rank}(\mathbf{A}\mathbf{B}) \leq \min\{\text{rank}(\mathbf{A}), \text{rank}(\mathbf{B})\}, \quad (52)$$

for arbitrary matrices $\mathbf{A} \in \mathbb{C}^{m \times k}$ and $\mathbf{B} \in \mathbb{C}^{k \times n}$. Combining the results in (51) and (52), we see that $\text{rank}(\mathbf{G}) = P$, and similarly, we can prove $\text{rank}(\mathbf{H}) = Q$.

APPENDIX B

In order to determine the conjugate gradient $\nabla_{\mathbf{X}_i^*} f_1$, we first compute the differential of f_1 with respect to \mathbf{X}_i^* . According to some basic differentiation rules for complex-valued matrices [38], we have

$$d(\|\mathbf{R} - \mathbf{X}\mathbf{F}\|_F^2) = -\text{tr}(\mathbf{F}d(\mathbf{X}^H)\mathbf{R} + \mathbf{F}^H d(\mathbf{X}^H)\mathbf{X}\mathbf{F}). \quad (53)$$

Besides, notice that $\|\boldsymbol{\lambda}_{\mathbf{X}}\|_1 = \sum_i \sum_j |[\mathbf{A}_{\text{BS}}^H \mathbf{X} \mathbf{A}_{\text{I}}]_{ij}|$, and therefore, defining the i -th column of \mathbf{A}_{BS} as \mathbf{a}_i and the j -th column of \mathbf{A}_{I} as \mathbf{b}_j , we have

$$\begin{aligned} & d(\|\boldsymbol{\lambda}_{\mathbf{X}}\|_1) \\ &= \sum_i \sum_j d\left(\left(\mathbf{b}_j^H \mathbf{X}^H \mathbf{a}_i \mathbf{a}_i^H \mathbf{X} \mathbf{b}_j\right)^{\frac{1}{2}}\right) = \frac{1}{2} \sum_i \sum_j \left(\mathbf{b}_j^H \mathbf{X}^H \mathbf{a}_i \mathbf{a}_i^H \mathbf{X} \mathbf{b}_j\right)^{-\frac{1}{2}} \mathbf{b}_j^H d(\mathbf{X}^H) \mathbf{a}_i \mathbf{a}_i^H \mathbf{X} \mathbf{b}_j \\ &= \frac{1}{2} \text{tr} \left(\sum_i \sum_j \mathbf{a}_i \mathbf{a}_i^H \mathbf{X} \mathbf{b}_j \left(\mathbf{b}_j^H \mathbf{X}^H \mathbf{a}_i \mathbf{a}_i^H \mathbf{X} \mathbf{b}_j\right)^{-\frac{1}{2}} \mathbf{b}_j^H d(\mathbf{X}^H) \right) = \frac{1}{2} \text{tr}(\mathbf{A}_{\text{BS}} \mathbf{Y} \mathbf{A}_{\text{I}}^H d(\mathbf{X}^H)), \end{aligned} \quad (54)$$

where \mathbf{Y} is defined in (23). Then, combining the results in (53) and (54), the differential of f_1 with respect to \mathbf{X}_i^* is given by

$$d(f_1) = \text{tr} \left(\left(-\mathbf{R}\mathbf{F}^H + \mathbf{X}\mathbf{F}\mathbf{F}^H + \frac{\mu_{\mathbf{G}}}{2} \mathbf{A}_{\text{BS}} \mathbf{Y} \mathbf{A}_{\text{I}}^H \right) d(\mathbf{X}^H) \right). \quad (55)$$

Finally, considering the fact that $d(f_1) = \text{tr}(\nabla_{\mathbf{X}_i^*} f_1 d(\mathbf{X}^H))$, the proof is completed.

REFERENCES

- [1] T. Lin, X. Yu, Y. Zhu, and R. Schober, "Channel estimation for intelligent reflecting surface-assisted millimeter wave MIMO systems," in *Proc. IEEE Global Commun. Conf. (GLOBECOM)*, Taipei, Taiwan, Dec. 2020, pp. 1–6.
- [2] Z. Pi and F. Khan, "An introduction to millimeter-wave mobile broadband systems," *IEEE Commun. Mag.*, vol. 49, no. 6, pp. 101–107, Jun. 2011.
- [3] P. Wang, Y. Li, L. Song, and B. Vucetic, "Multi-gigabit millimeter wave wireless communications for 5G: From fixed access to cellular networks," *IEEE Commun. Mag.*, vol. 53, no. 1, pp. 44 304–44 321, Jan. 2015.
- [4] S. Rangan, T. S. Rappaport, and E. Erkip, "Millimeter-wave cellular wireless networks: Potentials and challenges," *Proc. IEEE*, vol. 102, no. 3, pp. 366–385, Feb. 2014.
- [5] Q. Wu and R. Zhang, "Towards smart and reconfigurable environment: Intelligent reflecting surface aided wireless network," *IEEE Commun. Mag.*, vol. 58, no. 1, pp. 106–112, May 2020.
- [6] C. Huang, A. Zappone, G. C. Alexandropoulos, M. Debbah, and C. Yuen, "Reconfigurable intelligent surfaces for energy efficiency in wireless communication," *IEEE Trans. Wireless Commun.*, vol. 18, no. 8, pp. 4157–4170, Jun. 2019.
- [7] Q. Wu, S. Zhang, B. Zheng, C. You, and R. Zhang, "Intelligent reflecting surface aided wireless communications: A tutorial," *IEEE Trans. Commun.*, vol. 69, no. 5, pp. 3313–3351, Jan. 2021.
- [8] M. Nemati, J. Park, and J. Choi, "RIS-assisted coverage enhancement in millimeter-wave cellular networks," *IEEE Access*, vol. 8, pp. 188 171–188 185, Oct. 2020.
- [9] C. Pradhan, A. Li, L. Song, B. Vucetic, and Y. Li, "Hybrid precoding design for reconfigurable intelligent surface aided mmwave communication systems," *IEEE Wireless Commun. Lett.*, vol. 9, no. 7, pp. 1041–1045, Mar. 2020.
- [10] X. Yu, D. Xu, D. W. K. Ng, and R. Schober, "IRS-assisted green communication systems: Provable convergence and robust optimization," *IEEE Trans. Commun.*, pp. 1–1, Jun. 2021, to appear.
- [11] Z. Wang, L. Liu, and S. Cui, "Channel estimation for intelligent reflecting surface assisted multiuser communications: Framework, algorithms, and analysis," *IEEE Trans. Wireless Commun.*, vol. 19, no. 10, pp. 6607–6620, Jun. 2020.
- [12] T. L. Jensen and E. De Carvalho, "An optimal channel estimation scheme for intelligent reflecting surfaces based on a minimum variance unbiased estimator," in *Proc. IEEE Int. Conf. Acoust., Speech Signal Process. (ICASSP)*, Barcelona, Spain, May 2020, pp. 5000–5004.
- [13] J. Chen, Y.-C. Liang, H. V. Cheng, and W. Yu, "Channel estimation for reconfigurable intelligent surface aided multi-user MIMO systems," *arXiv preprint arXiv:1904.10136*, Dec. 2019.
- [14] A. Taha, M. Alrabeiah, and A. Alkhateeb, "Enabling large intelligent surfaces with compressive sensing and deep learning," *IEEE Access*, vol. 9, pp. 44 304–44 321, Mar. 2021.
- [15] H. Liu, X. Yuan, and Y. J. A. Zhang, "Matrix-calibration-based cascaded channel estimation for reconfigurable intelligent surface assisted multiuser MIMO," *IEEE J. Sel. Areas Commun.*, vol. 38, no. 11, pp. 2621–2636, Jul. 2020.
- [16] Z. He and X. Yuan, "Cascaded channel estimation for large intelligent metasurface assisted massive MIMO," *IEEE Wireless Commun. Lett.*, vol. 9, no. 2, pp. 210–214, Oct. 2019.
- [17] J. He, M. Leinonen, H. Wymeersch, and M. Juntti, "Channel estimation for RIS-aided mmwave MIMO systems," in *Proc. IEEE Global Commun. Conf. (GLOBECOM)*, Taipei, Taiwan, Dec. 2020, pp. 1–6.
- [18] G. T. de Araújo, A. L. F. de Almeida, and R. Boyer, "Channel estimation for intelligent reflecting surface assisted MIMO systems: A tensor modeling approach," *IEEE J. Sel. Topics Signal Process.*, vol. 15, no. 3, pp. 789–802, Feb. 2021.
- [19] L. Wei, C. Huang, G. C. Alexandropoulos, and C. Yuen, "Parallel factor decomposition channel estimation in RIS-assisted multi-user MISO communication," in *Proc. IEEE Sensor Array Multichannel Signal Process. Workshop (SAM)*, Hangzhou, China, Jun. 2020, pp. 1–5.
- [20] P. Wang, J. Fang, H. Duan, and H. Li, "Compressed channel estimation for intelligent reflecting surface-assisted millimeter wave systems," *IEEE Signal Process. Lett.*, vol. 27, pp. 905–909, May 2020.

- [21] X. Ma, Z. Chen, W. Chen, Z. Li, Y. Chi, C. Han, and S. Li, "Joint channel estimation and data rate maximization for intelligent reflecting surface assisted terahertz MIMO communication systems," *IEEE Access*, vol. 8, pp. 99 565–99 581, May 2020.
- [22] C. Pan, H. Ren, K. Wang, W. Xu, M. ElKashlan, A. Nallanathan, and L. Hanzo, "Multicell MIMO communications relying on intelligent reflecting surfaces," *IEEE Trans. Wireless Commun.*, vol. 19, no. 8, pp. 5218–5233, Jul. 2020.
- [23] P. Wang, J. Fang, L. Dai, and H. Li, "Joint transceiver and large intelligent surface design for massive MIMO mmWave systems," *IEEE Trans. Wireless Commun.*, vol. 20, no. 2, pp. 1052–1064, Feb. 2021.
- [24] J. Lee, G. Gil, and Y. H. Lee, "Channel estimation via orthogonal matching pursuit for hybrid MIMO systems in millimeter wave communications," *IEEE Trans. Commun.*, vol. 64, no. 6, pp. 2370–2386, May 2016.
- [25] X. Yu, D. Xu, Y. Sun, D. W. K. Ng, and R. Schober, "Robust and secure wireless communications via intelligent reflecting surfaces," *IEEE J. Sel. Areas Commun.*, vol. 38, no. 11, pp. 2637–2652, Jul. 2020.
- [26] X. Li, J. Fang, H. Li, and P. Wang, "Millimeter wave channel estimation via exploiting joint sparse and low-rank structures," *IEEE Trans. Wireless Commun.*, vol. 17, no. 2, pp. 1123–1133, Jul. 2018.
- [27] C. R. Berger, Z. Wang, J. Huang, and S. Zhou, "Application of compressive sensing to sparse channel estimation," *IEEE Commun. Mag.*, vol. 48, no. 11, pp. 164–174, Nov. 2010.
- [28] X. Yu, J.-C. Shen, J. Zhang, and K. B. Letaief, "Alternating minimization algorithms for hybrid precoding in millimeter wave MIMO systems," *IEEE J. Sel. Topics Signal Process.*, vol. 10, no. 3, pp. 485–500, Apr. 2016.
- [29] H. Guo, Y. Liang, J. Chen, and E. G. Larsson, "Weighted sum-rate maximization for reconfigurable intelligent surface aided wireless networks," *IEEE Trans. Wireless Commun.*, vol. 19, no. 5, pp. 3064–3076, May. 2020.
- [30] Z. Li, M. Hua, Q. Wang, and Q. Song, "Weighted sum-rate maximization for multi-IRS aided cooperative transmission," *IEEE Wireless Commun. Lett.*, vol. 9, no. 10, pp. 1620–1624, Oct. 2020.
- [31] N. Boumal, "An introduction to optimization on smooth manifolds," Available online, Nov 2020. [Online]. Available: <http://www.nicolasboumal.net/book>
- [32] P.-A. Absil, R. Mahony, and R. Sepulchre, *Optimization algorithms on matrix manifolds*. Princeton University Press, 2009.
- [33] J. R. Shewchuk, "An introduction to the conjugate gradient method without the agonizing pain," 1994.
- [34] O. E. Ayach, S. Rajagopal, S. Abu-Surra, Z. Pi, and R. W. Heath, "Spatially sparse precoding in millimeter wave MIMO systems," *IEEE Trans. Wireless Commun.*, vol. 13, no. 3, pp. 1499–1513, Mar. 2014.
- [35] X. Zhang, *Matrix analysis and applications*, Cambridge Univ. Press, 2017.
- [36] S. S. Christensen, R. Agarwal, E. De Carvalho, and J. M. Cioffi, "Weighted sum-rate maximization using weighted MMSE for MIMO-BC beamforming design," *IEEE Trans. Wireless Commun.*, vol. 7, no. 12, pp. 4792–4799, Dec. 2008.
- [37] T. Lin, J. Cong, Y. Zhu, J. Zhang, and K. B. Letaief, "Hybrid beamforming for millimeter wave systems using the MMSE criterion," *IEEE Trans. Commun.*, vol. 67, no. 5, pp. 3693–3708, May 2019.
- [38] A. Hjørungnes, *Complex-Valued Matrix Derivatives*, Cambridge, U.K.: Cambridge Univ. Press, 2011.
- [39] G. Zhou, C. Pan, H. Ren, P. Popovski, and A. L. Swindlehurst, "Channel estimation for RIS-aided multiuser millimeter-wave systems," *arXiv preprint arXiv:2106.14792*, Jul. 2021.
- [40] P. Wang, J. Fang, X. Yuan, Z. Chen, and H. Li, "Intelligent reflecting surface-assisted millimeter wave communications: Joint active and passive precoding design," *IEEE Trans. Veh. Technol.*, vol. 69, no. 12, pp. 14 960–14 973, Oct. 2020.